A Photoionization Method for Black Hole Mass Estimation in Quasars☆

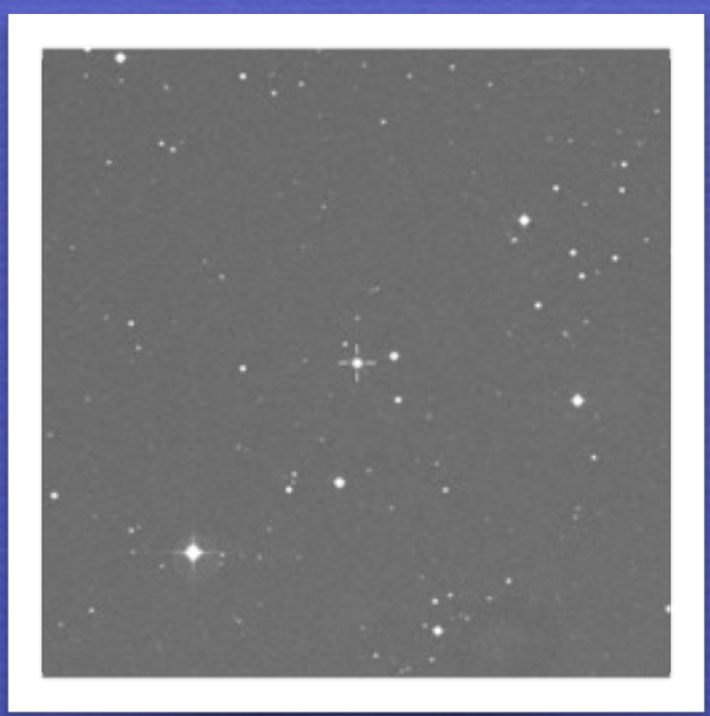

3C 273, z=0.158

Paola Marziani, INAF, Osservatorio Astronomico di Padova, Italia

with

C. Alenka Negrete (IA-UNAM), Deborah Dultzin (IA-UNAM), Jack W. Sulentic (IAA-CSIC)

☆*Based in part on C. A. Negrete's doctoral thesis*

Accretion onto a massive compact object

Physics

Black hole mass ($M_{\rm BH}$)

Accretion rate ($L_{\rm bol}$)

Eddington ratio ($L_{\rm bol}/M_{\rm BH}$)

Gas chemical composition

Black hole spin (radio-loudness)

Host galaxy morphology

Aspect

Viewing angle

Virial Black Hole Mass

geometry
dynamics

$$M_{\rm BH} = \frac{fr(\delta v)^2}{G}$$

$r_{\rm BLR}$

FHWM
σ, FWZI

$$M_{\rm BH} : \text{if } \delta v = \text{FWHM, isotropy} : \frac{\sqrt{3}}{2}\text{FWHM} \rightarrow f = 0.75$$

Keplerian velocity field: the BLR dynamics dominated by the gravity of a central mass; $v \propto r^{-1/2}$

The broad line emitting region not resolved...

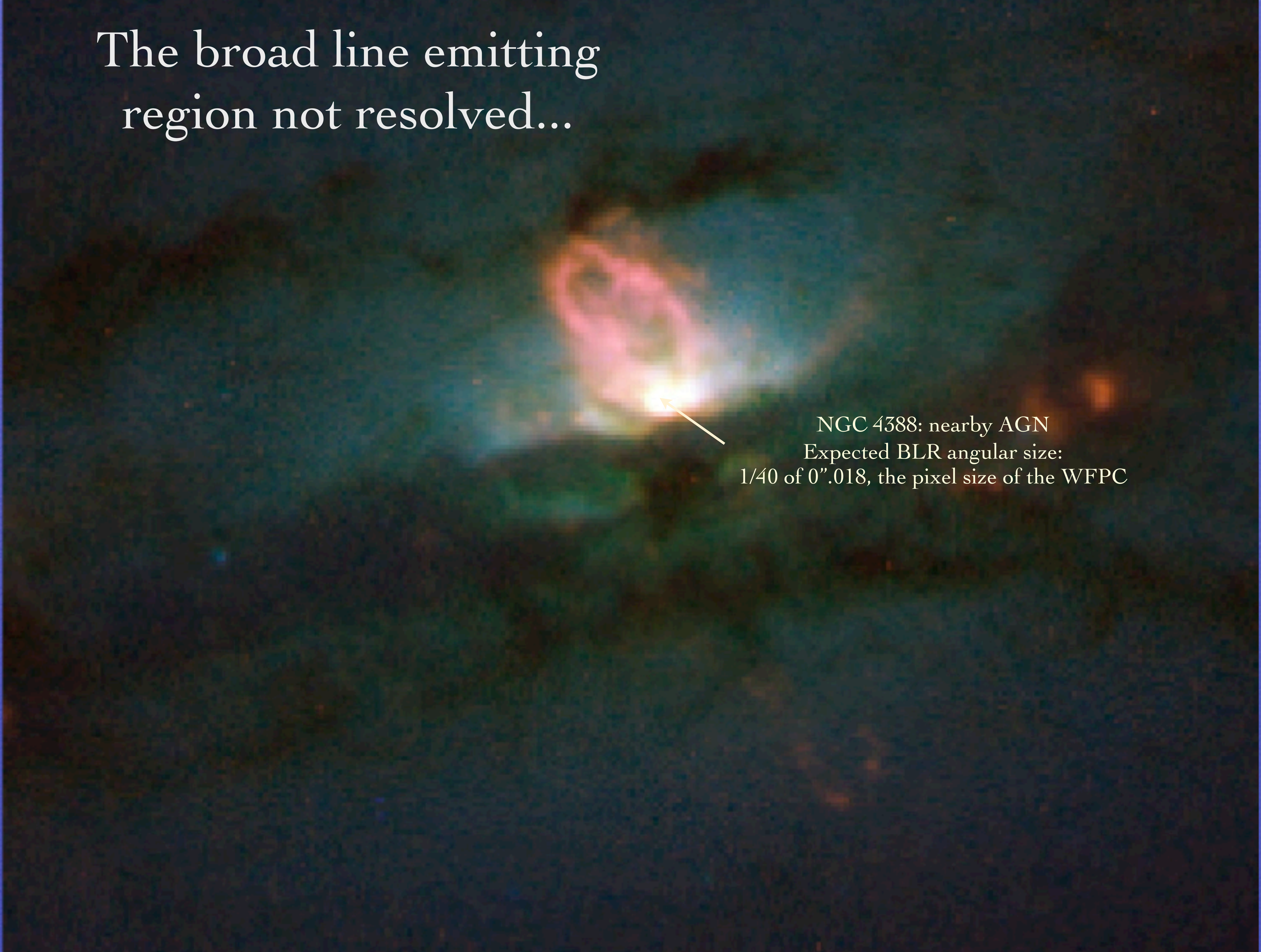

The emission lines

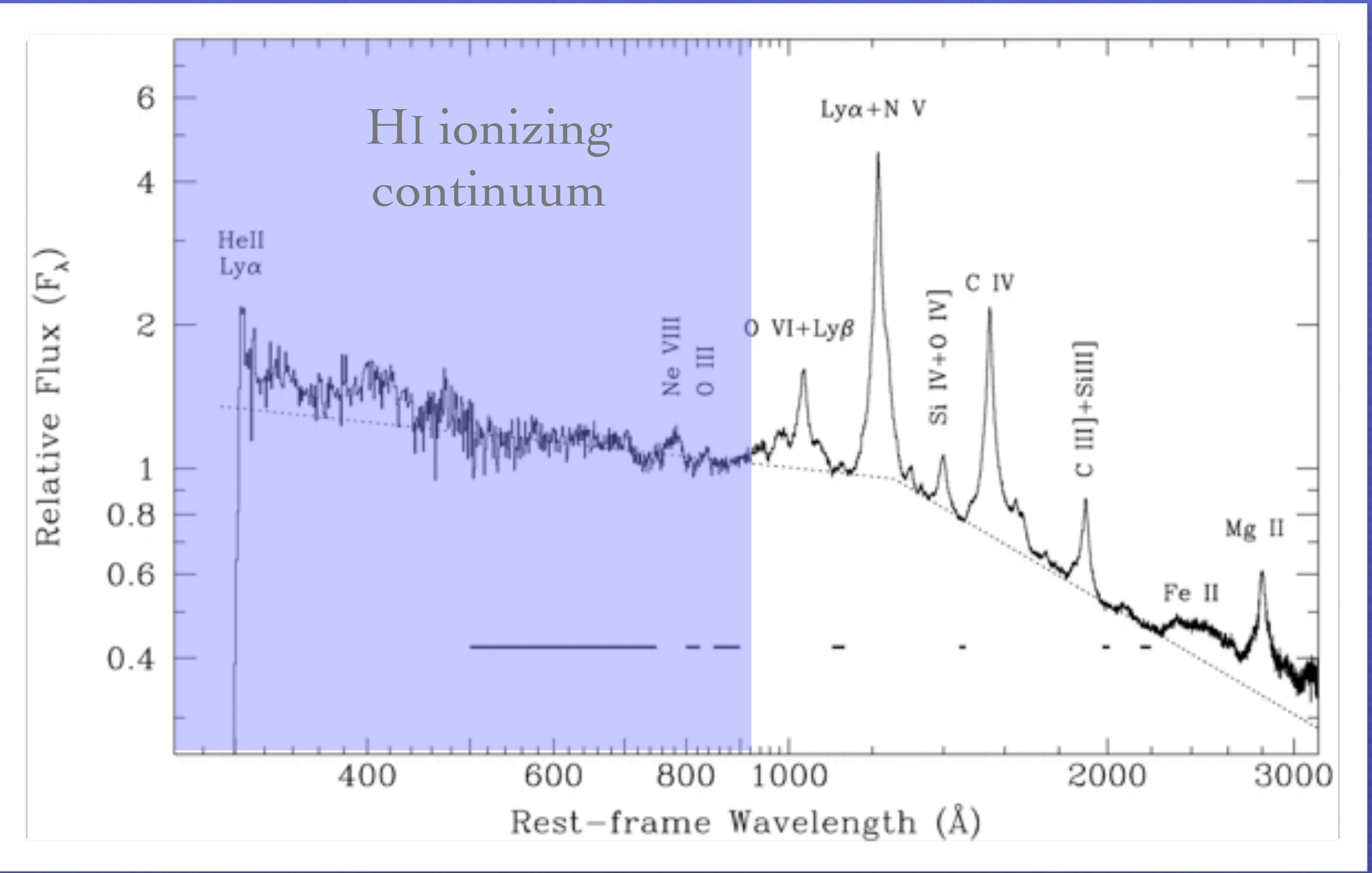

Telfer et al. 2002

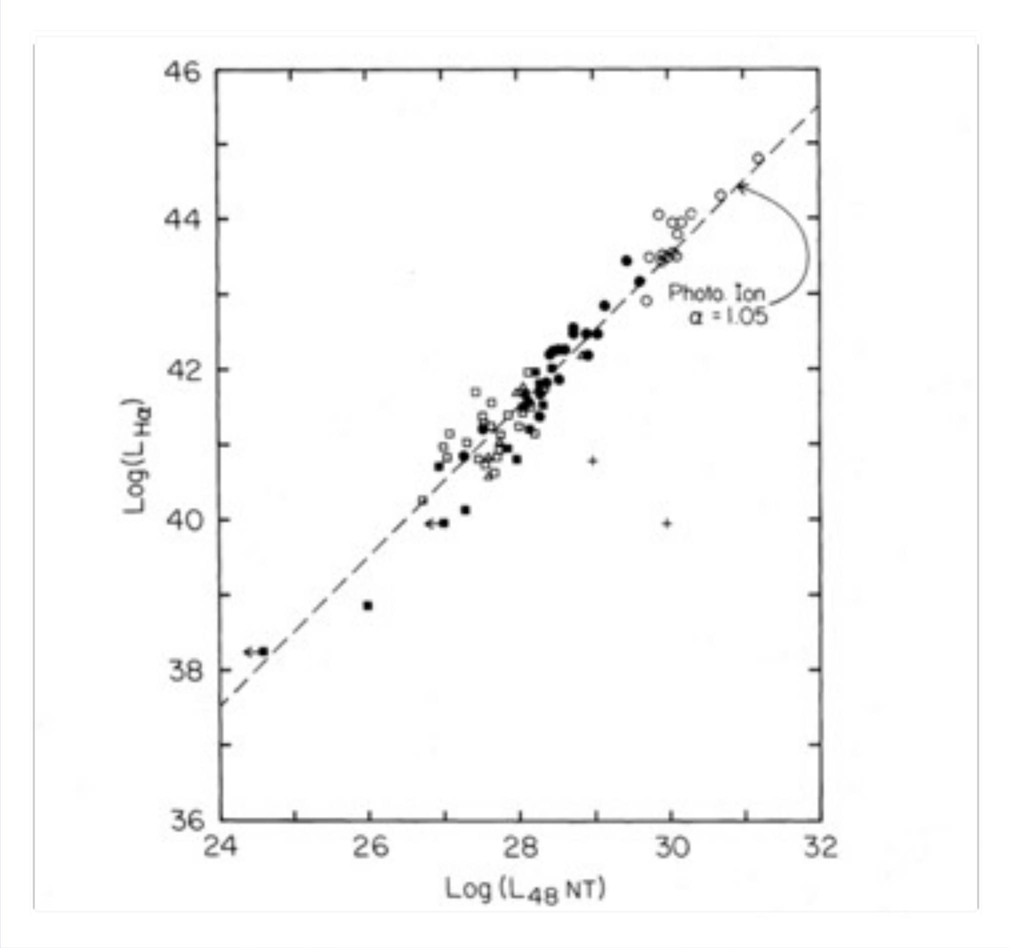

Shuder 1981

Photoionization by FUV continuum

Line luminosity proportional
to continuum luminosity;
Lines respond to continuum luminosity change

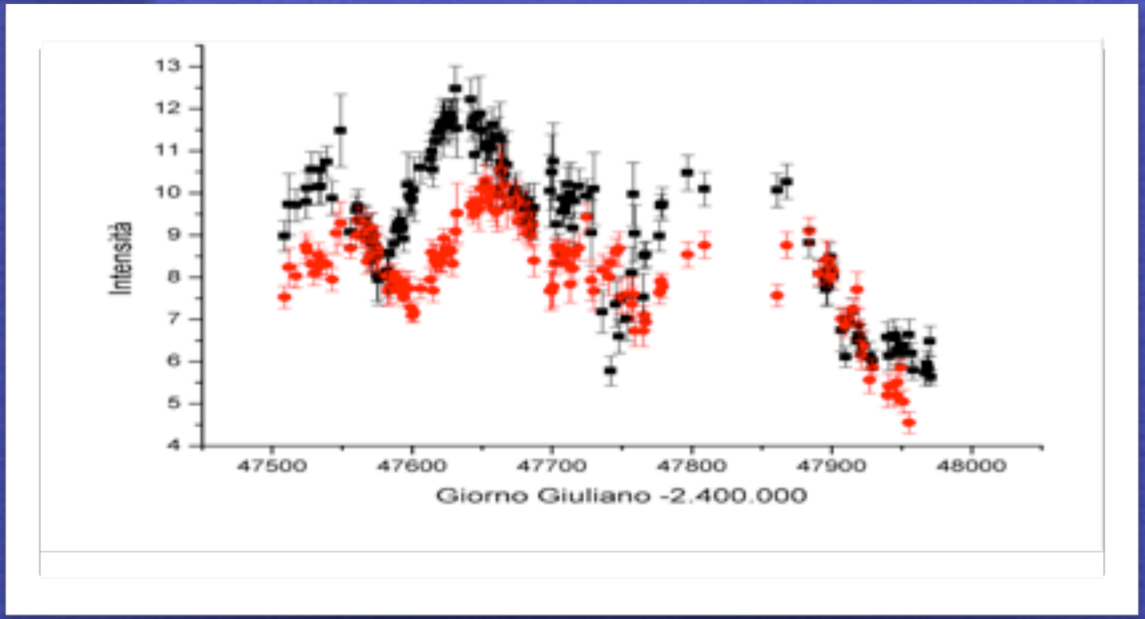

B. Peterson & the International AGN Watch

Test of virial relationship

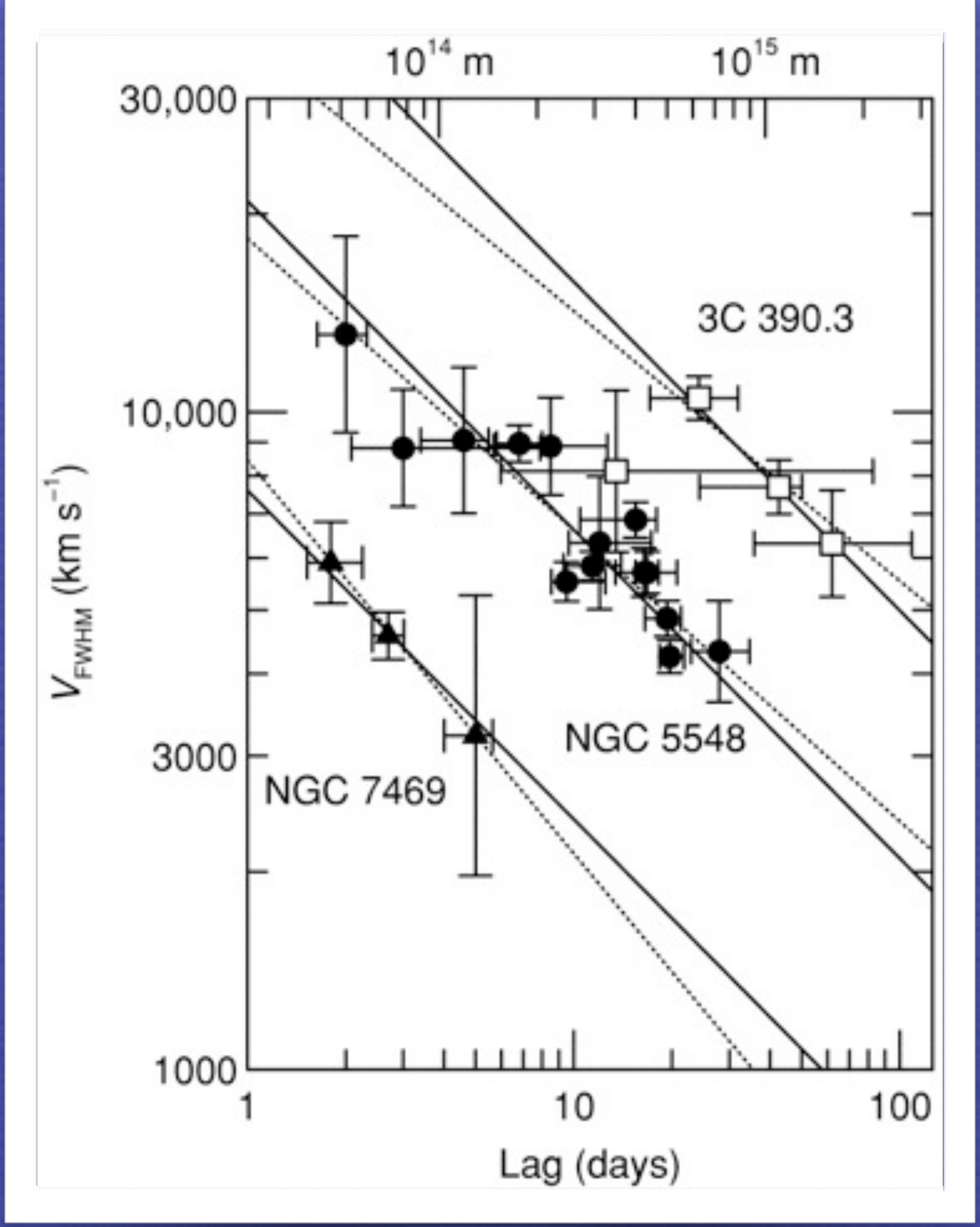

Peterson & Wandel

Peterson et al. 2004

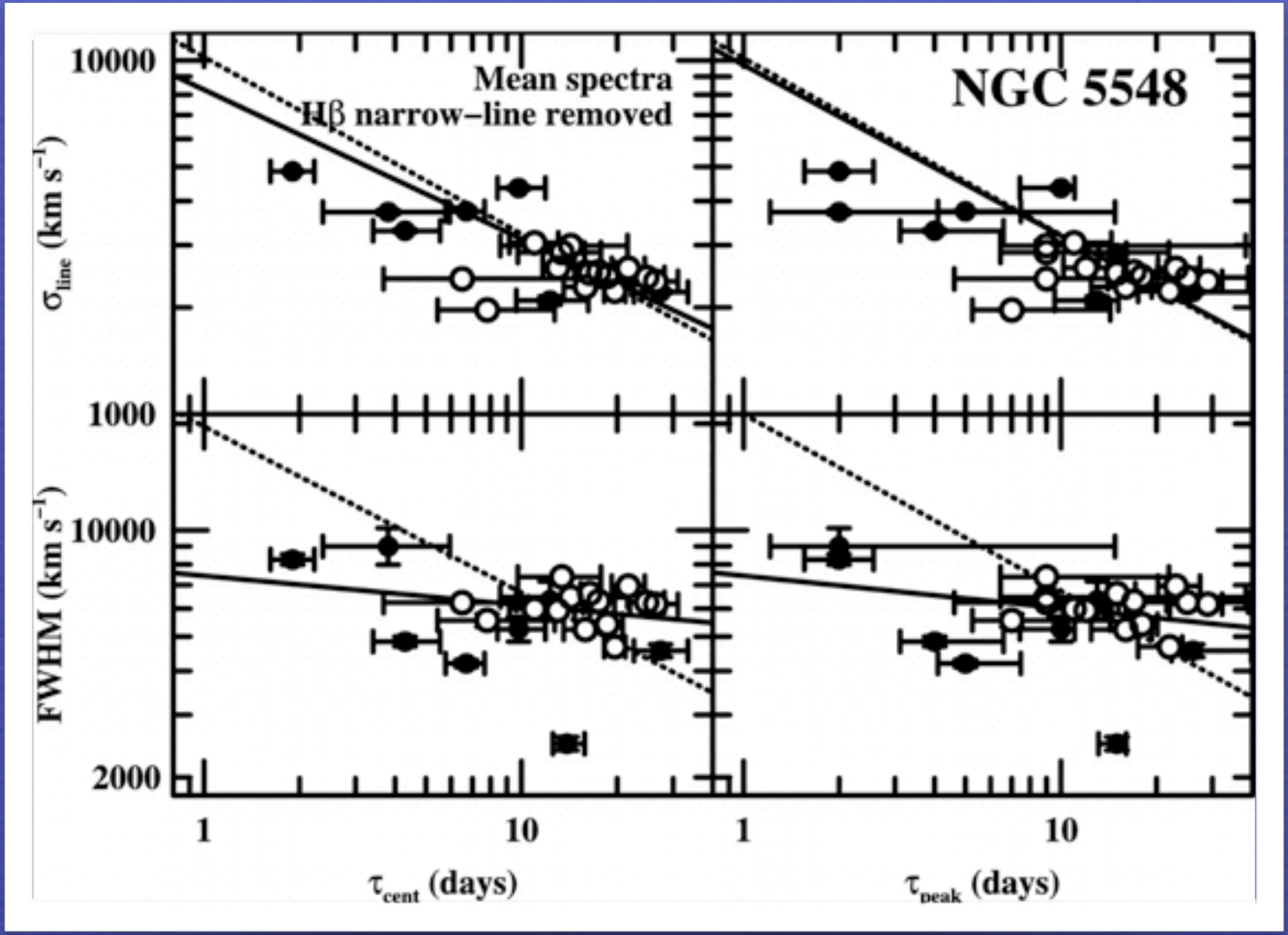

Best consistence with virial for rms and σ

Emitting region distance $r_{\rm BLR}$ from central continuum source

Peak or (centroid) of the cross-correlation function between line and continuum

$$\mathrm{CCF}(\tau) = \int \mathcal{L}(t)\mathcal{C}(t-\tau)dt$$

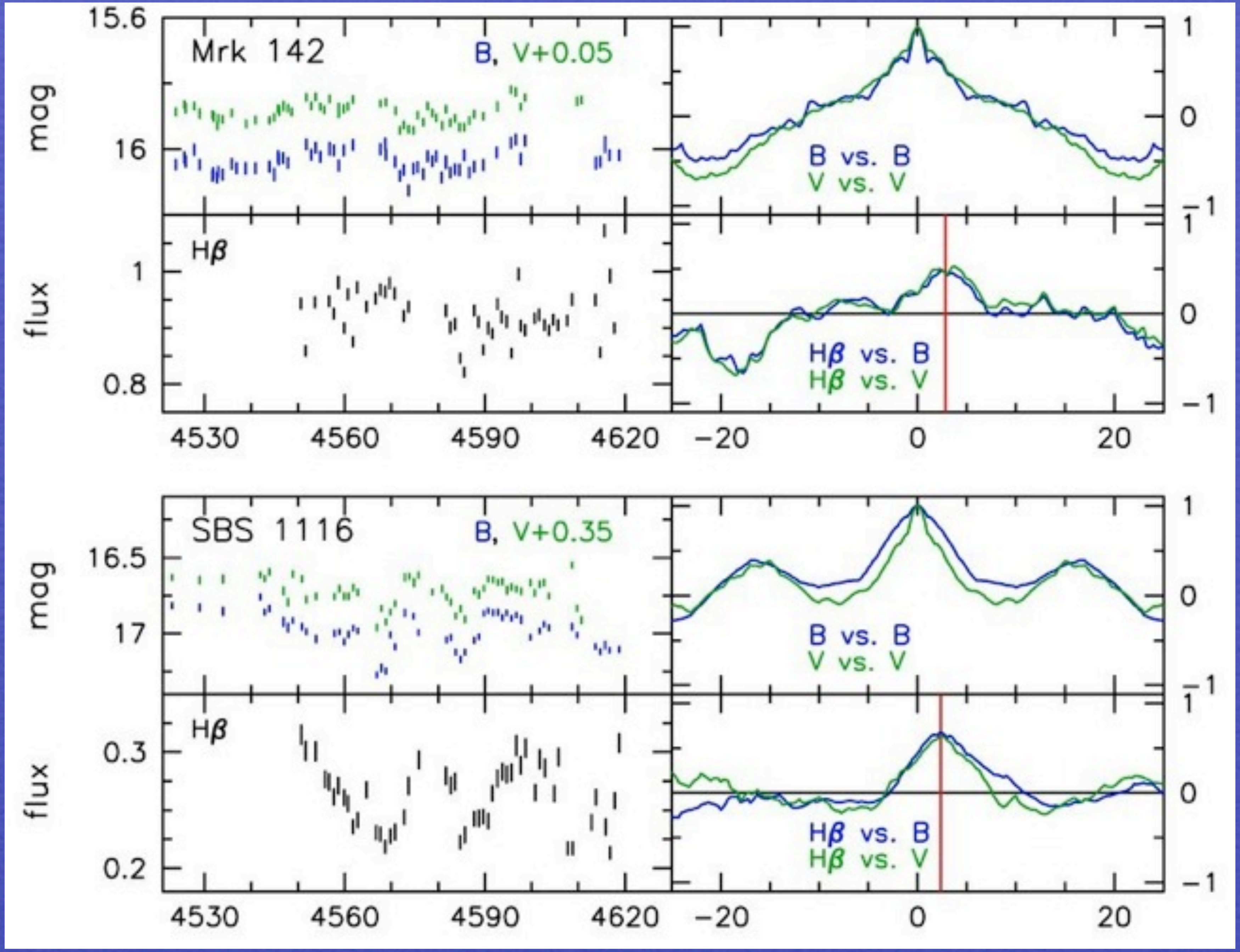

$r_{\rm BLR} = c\tau_{\rm H\beta}$

from Hβ monitoring is available for ~50 low-z AGN as of Dec. 2010

(Kaspi et al., Bentz. et al. 2009)

r_{BLR} indirect ("secondary") determination from Hβ

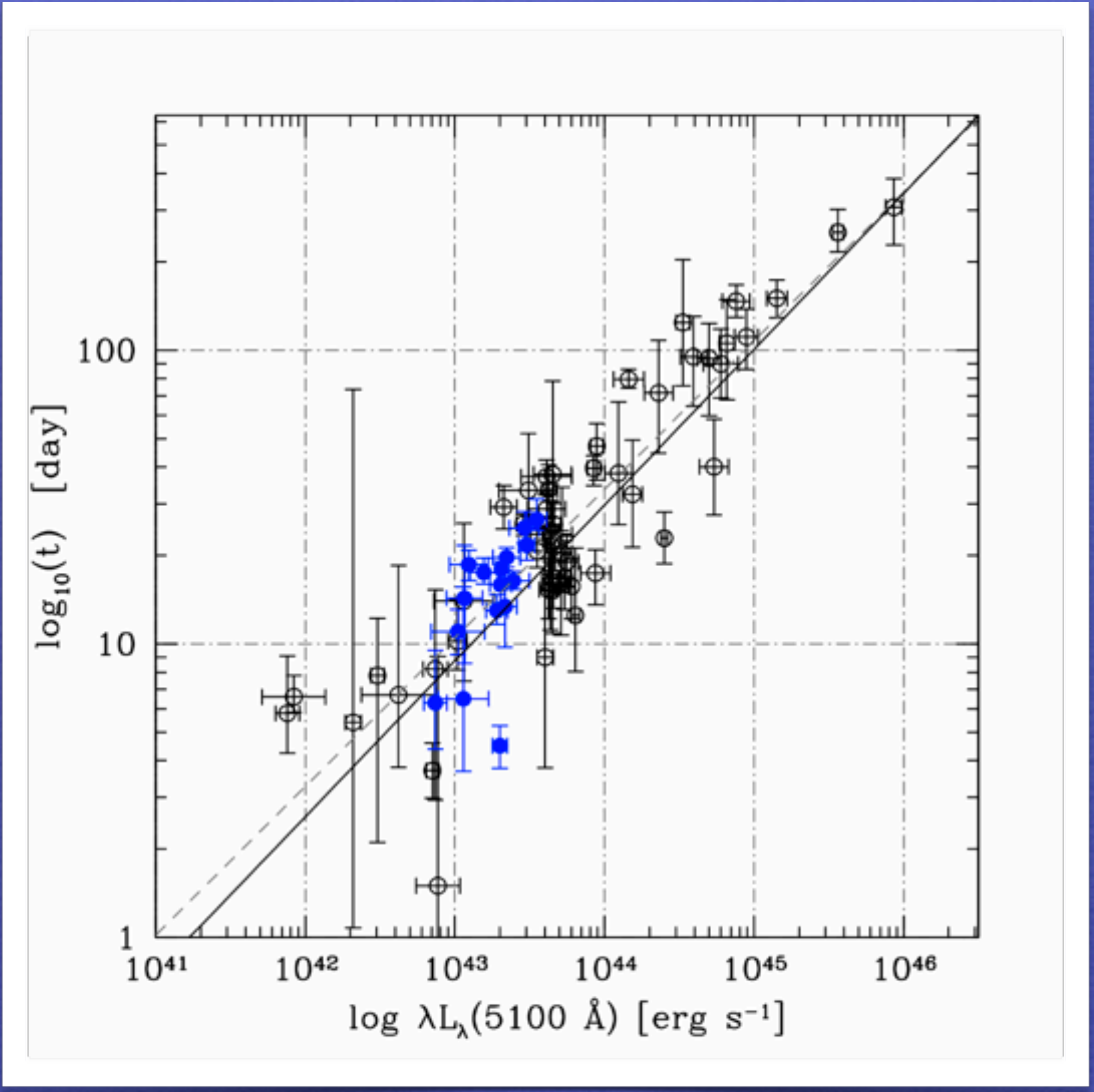

(all determinations data from Bentz. et al. 2009; cf. Kaspi et al., 2000,2005)

r_{BLR} correlates with L^a

a ~ 0.5 - 0.7, with a ≈ 0.52 now favored

Continuum luminosity is affecting the response time

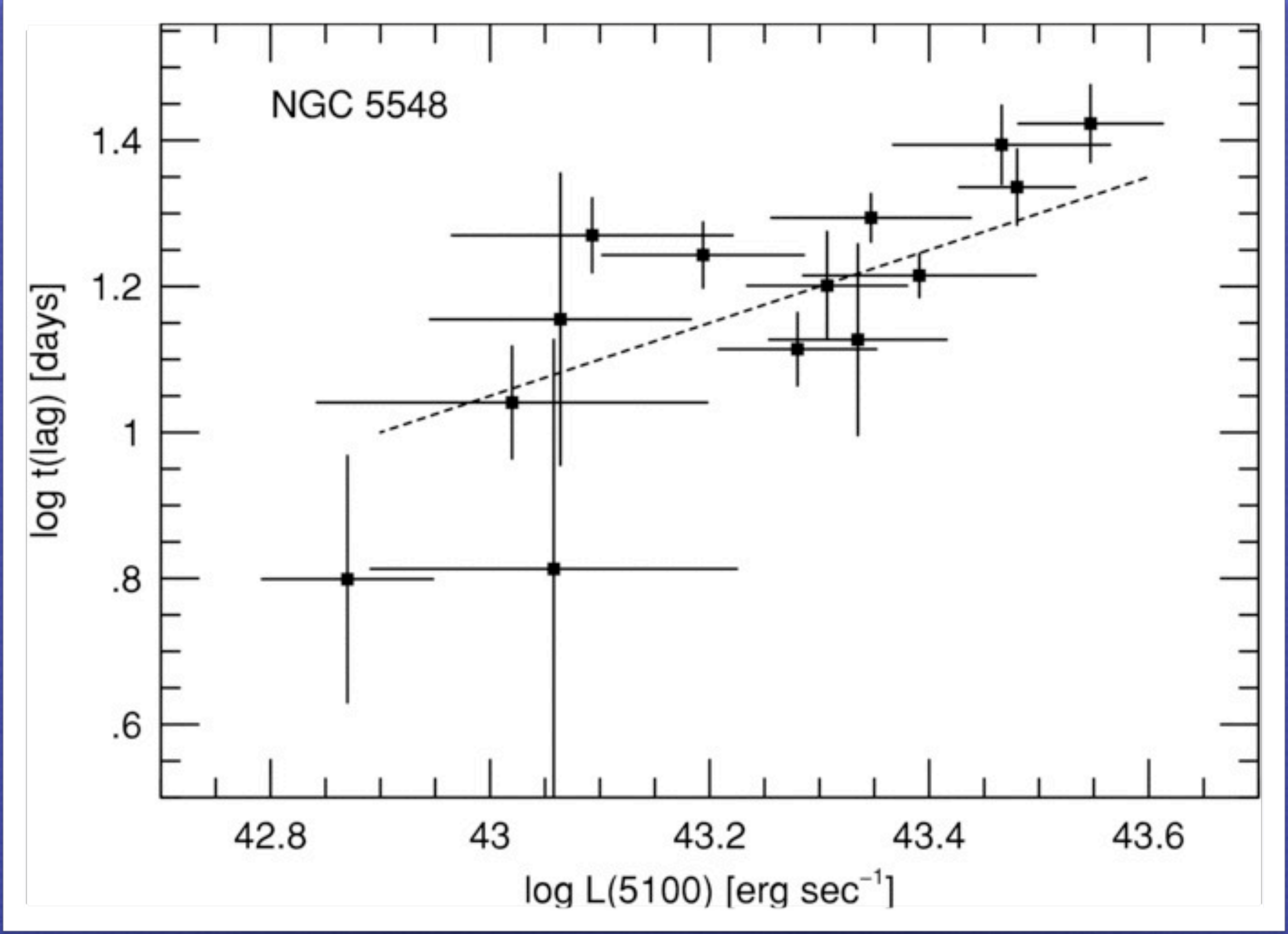

Netzer & Marziani 2010

Effect of radiation pressure on f on a system of clouds

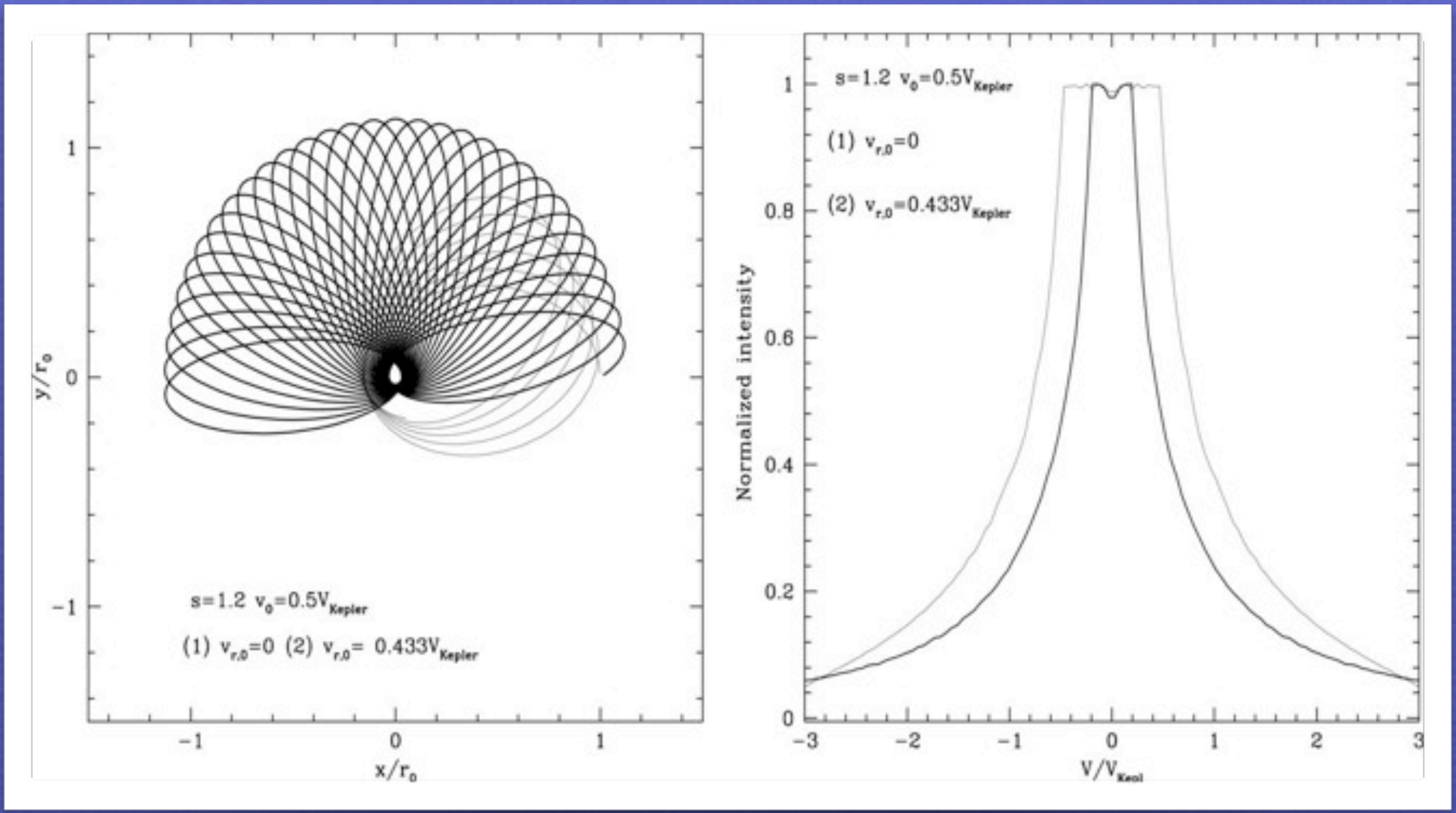

Netzer & Marziani 2010

$$M_{\rm BH} = f\, r\, (\delta v)^2\, G^{-1}$$

Table 1
Line Widths, Mass Conversion Factor f, and Emissivity-weighted Radii for Various Models Assuming the Line Emissivity is Strictly Proportional to the Cloud Cross Section and $\alpha(r) = 0.5$

Γ	FWHM/$v_{\rm Kepler}(r_0)$	$\langle r\rangle/r_0$	f
$s = 1.2$	$r_{23} = 10r_0$	$v_0 = 0.5$	
0.05	1.58 (0.93)	0.54	0.75 (2.18)
0.1	1.55 (0.92)	0.54	0.77 (2.21)
0.3	1.45 (0.87)	0.56	0.85 (2.37)
0.5	1.34 (0.81)	0.59	0.94 (2.56)
0.7	1.15 (0.72)	0.68	1.11 (2.78)
0.735	1.06 (0.68)	0.78	1.13 (2.76)

M_{BH} vs. bulge stellar velocity dispersion

Geometry factor f obtained scaling the M_{BH} to agree with the dynamical masses

Results have varied widely: f(FWHM)≈2
Woo et al. 2010

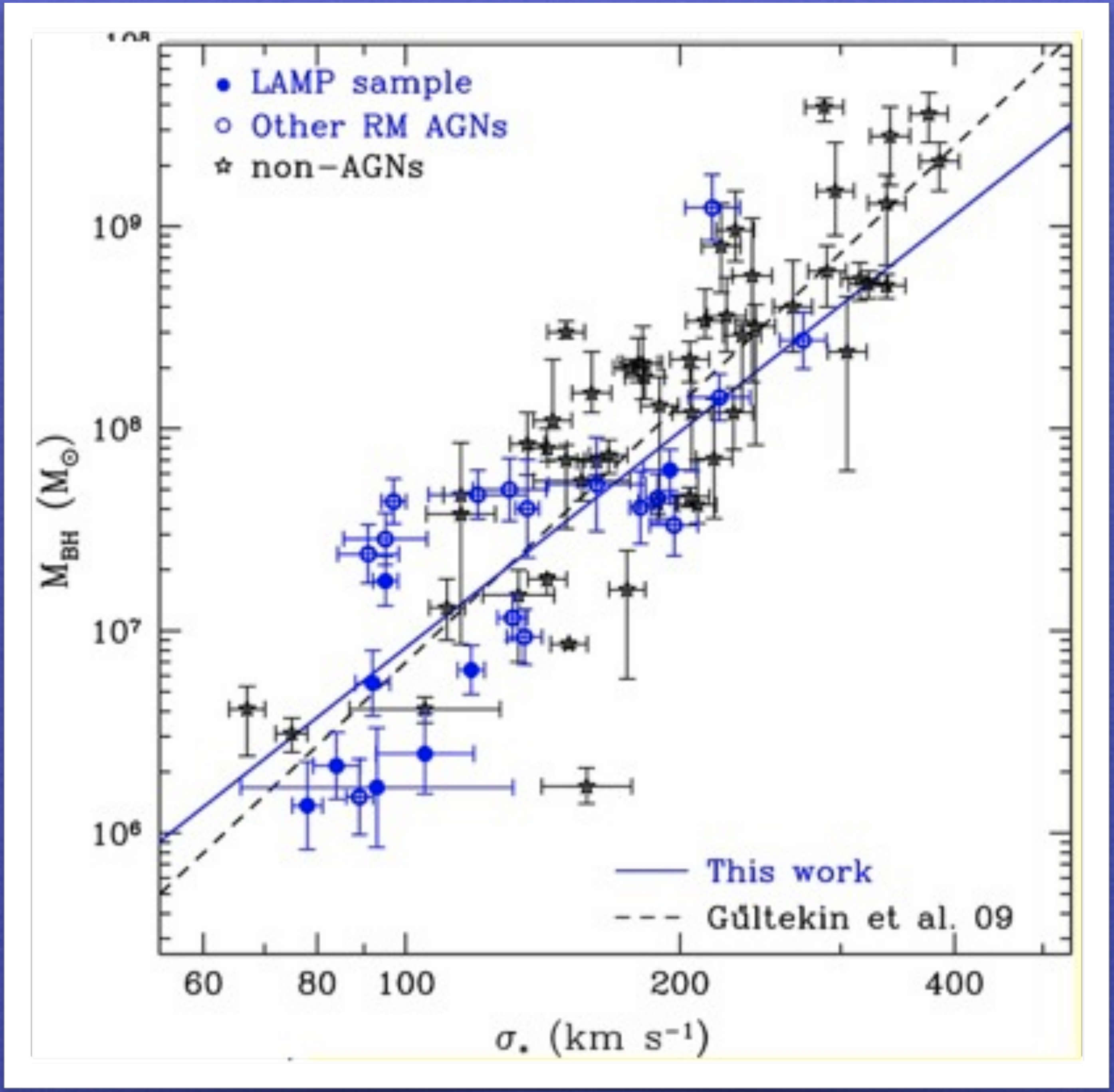

Woo et al. 2010; cf Gültekin et al. 2009;
Onken et al. 2004; Ferrarere & Merritt 2000; also Graham et al. 2011

f is most likely dependent on profile shape

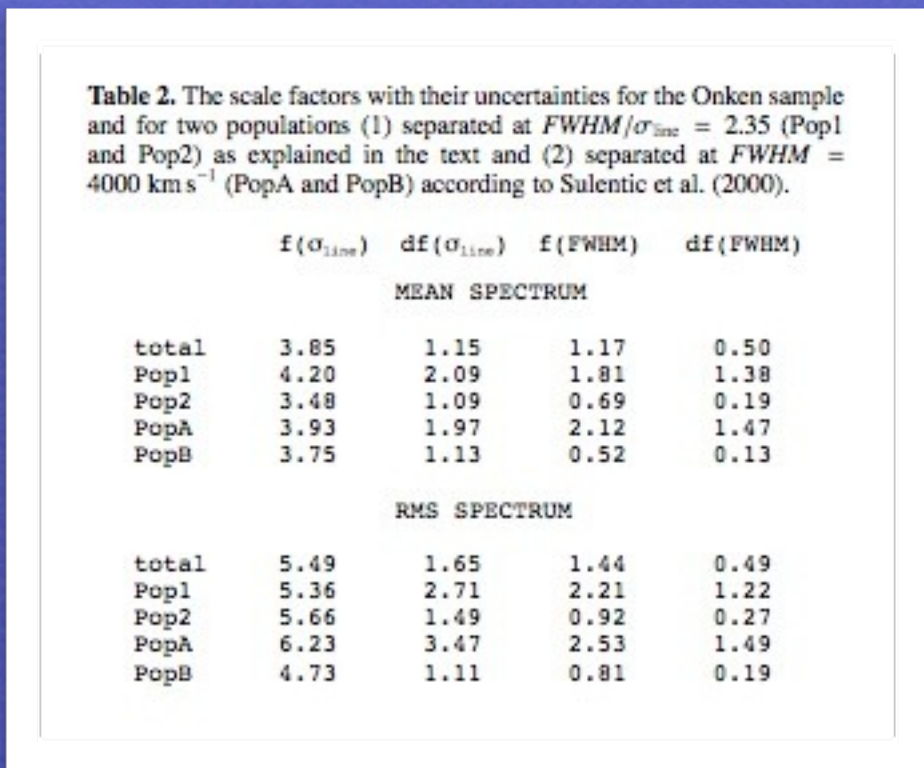

Table 2. The scale factors with their uncertainties for the Onken sample and for two populations (1) separated at $FWHM/\sigma_{line}$ = 2.35 (Pop1 and Pop2) as explained in the text and (2) separated at $FWHM$ = 4000 km s^{-1} (PopA and PopB) according to Sulentic et al. (2000).

	$f(\sigma_{line})$	$df(\sigma_{line})$	f(FWHM)	df(FWHM)
		MEAN SPECTRUM		
total	3.85	1.15	1.17	0.50
Pop1	4.20	2.09	1.81	1.38
Pop2	3.48	1.09	0.69	0.19
PopA	3.93	1.97	2.12	1.47
PopB	3.75	1.13	0.52	0.13
		RMS SPECTRUM		
total	5.49	1.65	1.44	0.49
Pop1	5.36	2.71	2.21	1.22
Pop2	5.66	1.49	0.92	0.27
PopA	6.23	3.47	2.53	1.49
PopB	4.73	1.11	0.81	0.19

Collin et al. 2006

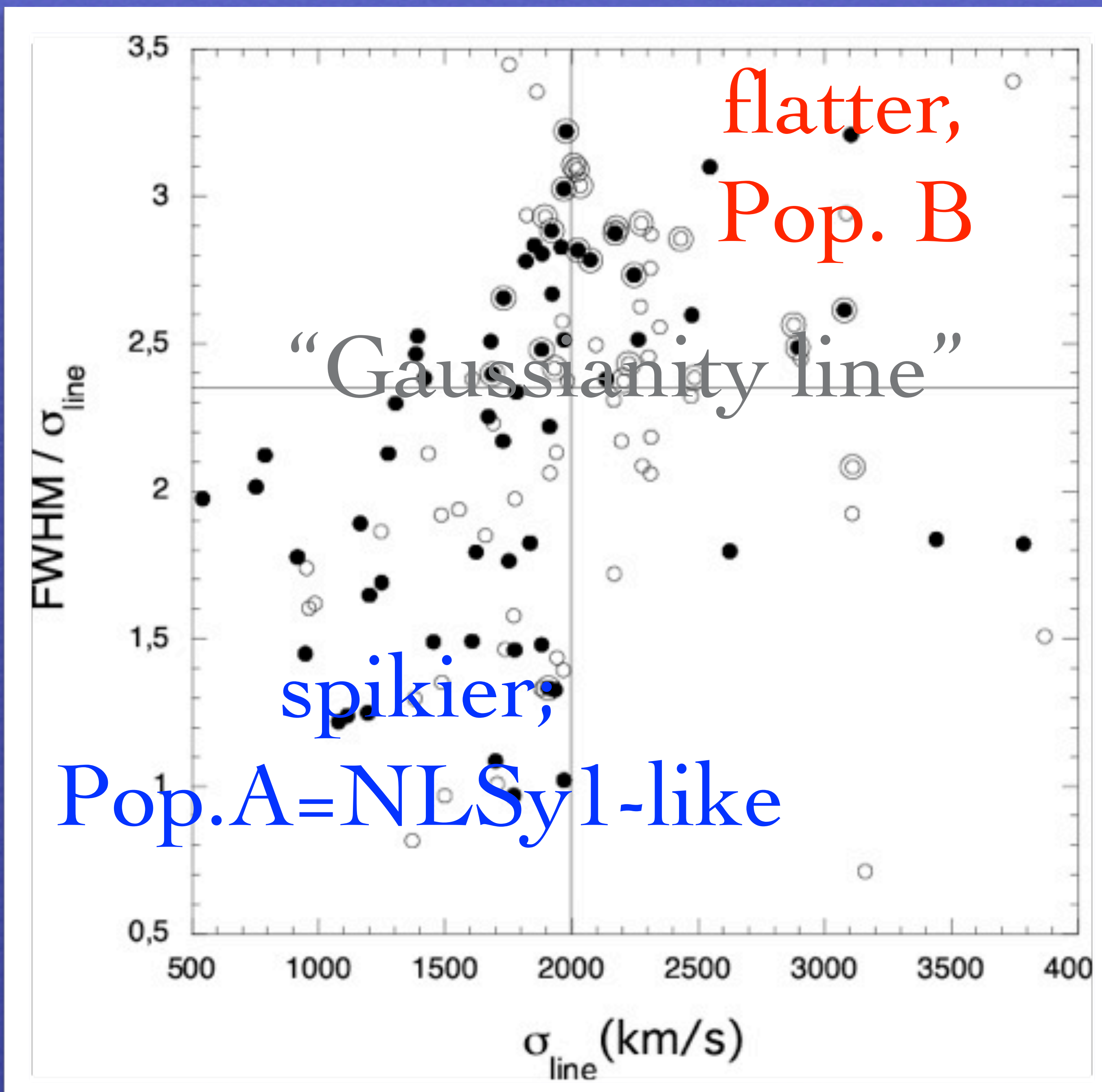

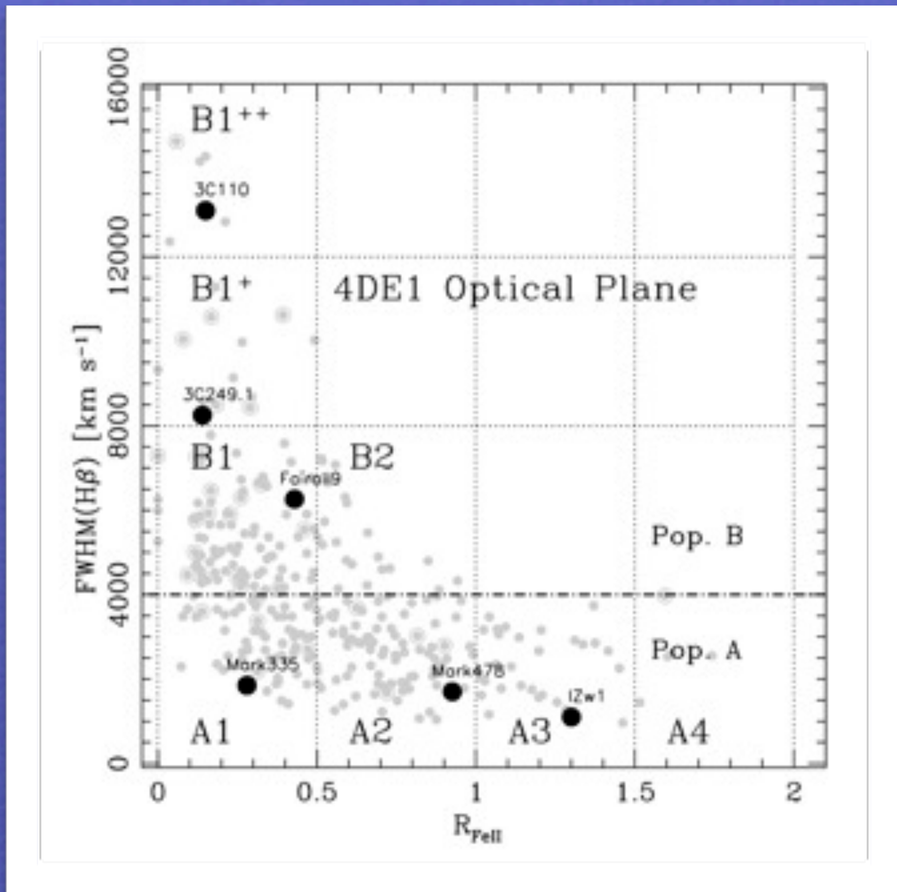

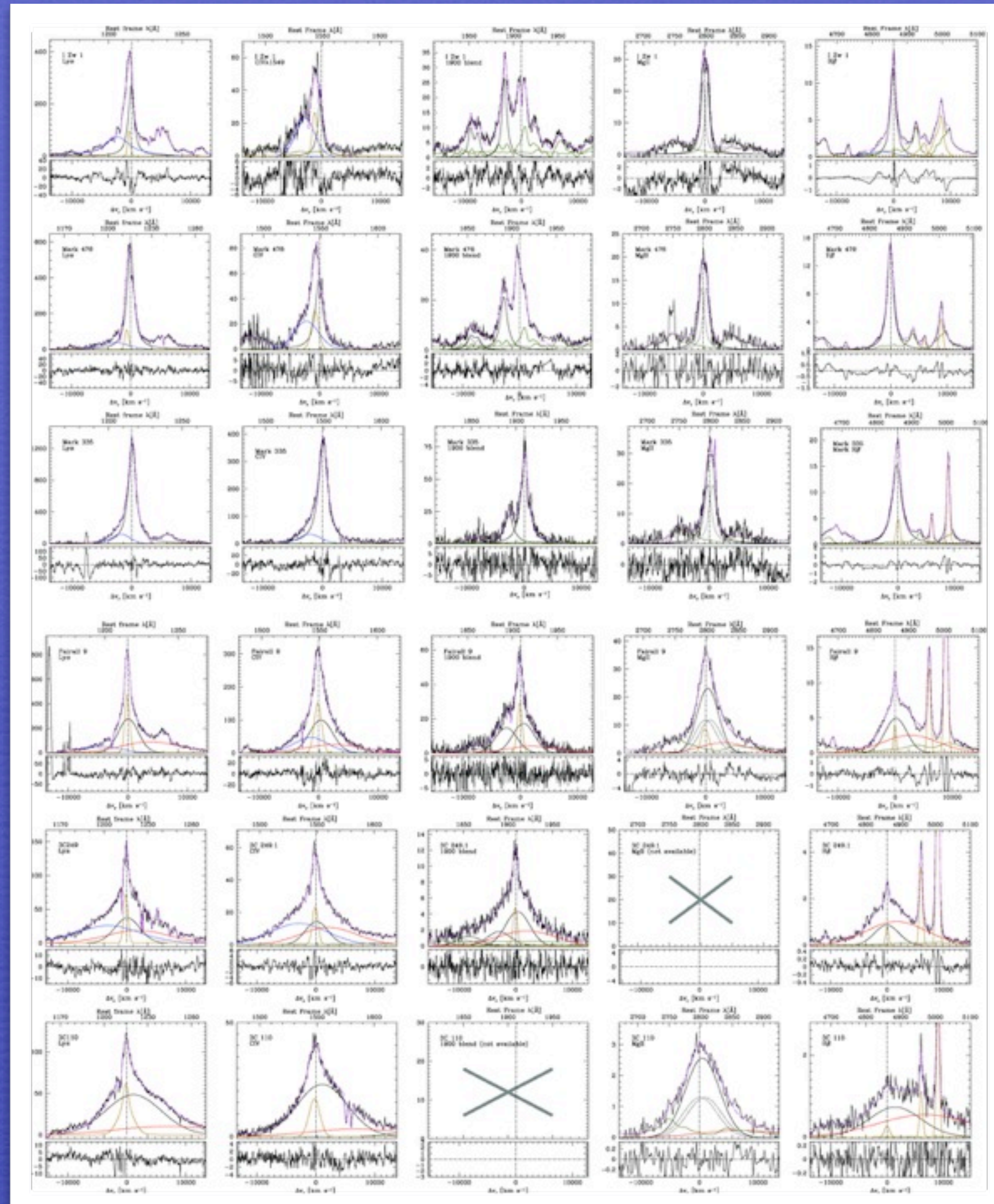

Blueshifted component: strong in Lyα, CIVλ1549, HeIIλ1640

"Broad Component": strong in all Low ionization lines: FeII, AlIIIλ1860, MgIIλ2800, Hβ

"Very Broad Component": strong in Lyα, CIVλ1549, Balmer lines of Population B sources only; absent in FeII

Marziani et al. 2010

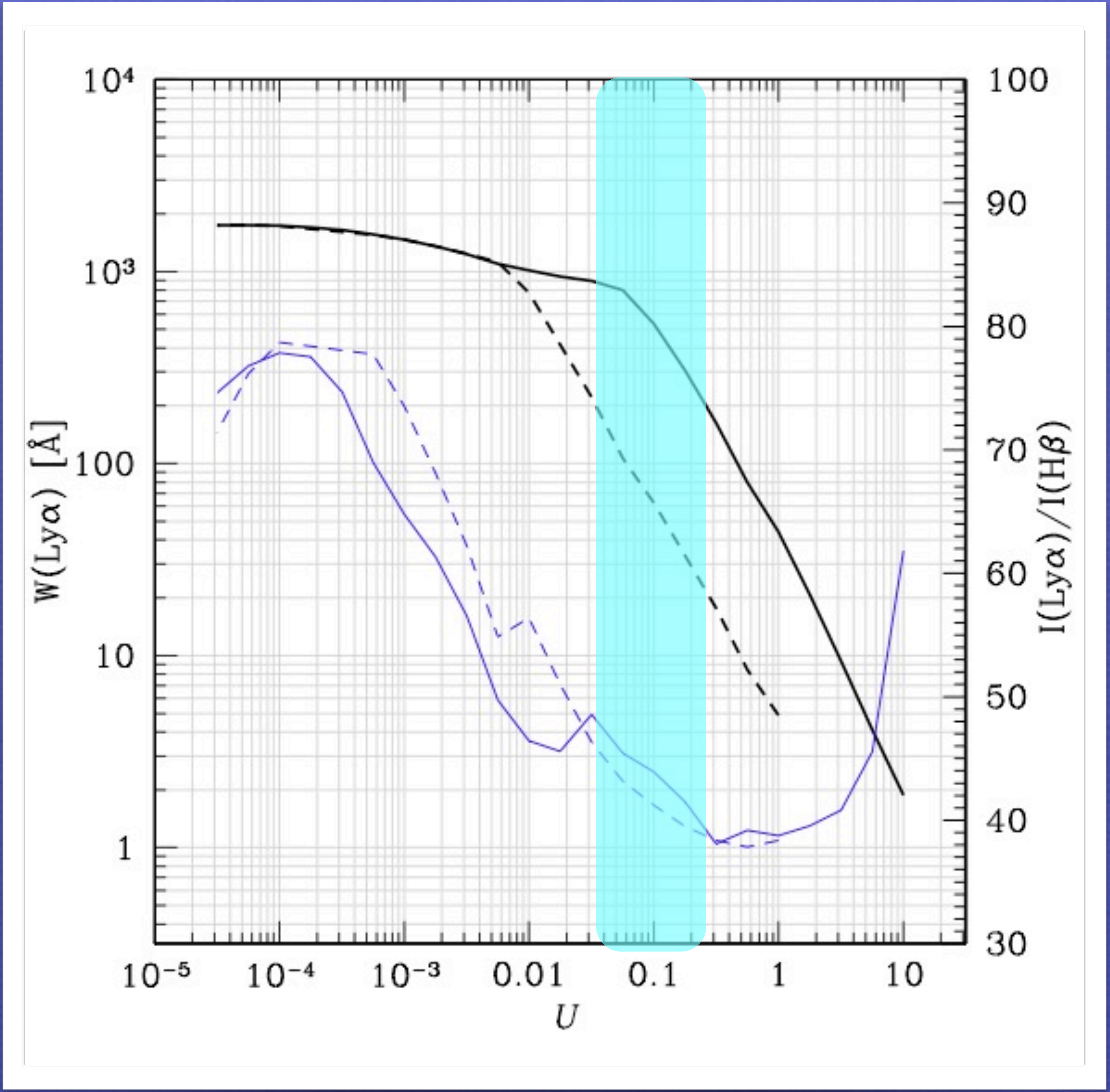

Blueshifted component: large Lyα/Hβ

Hβ detected only in median spectra or in extreme objects

Very different from the other components for which Lyα/Hβ ~ 5 – 10

$$U = \frac{\text{number density of ionizing photons}}{\text{electron density}}$$

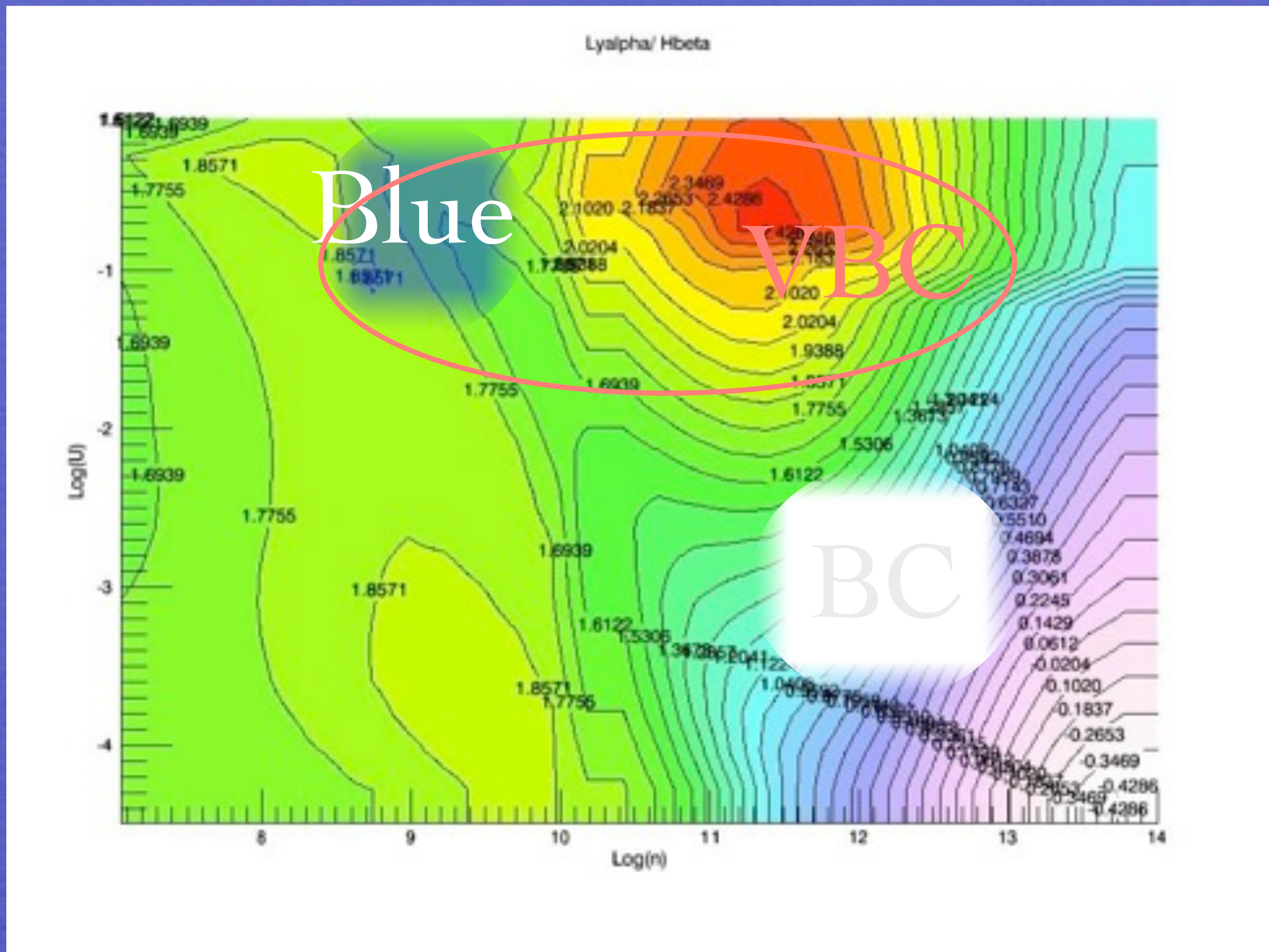
Lyalpha/ Hbeta
Blue
VBC
BC
Log(U)
Log(n)

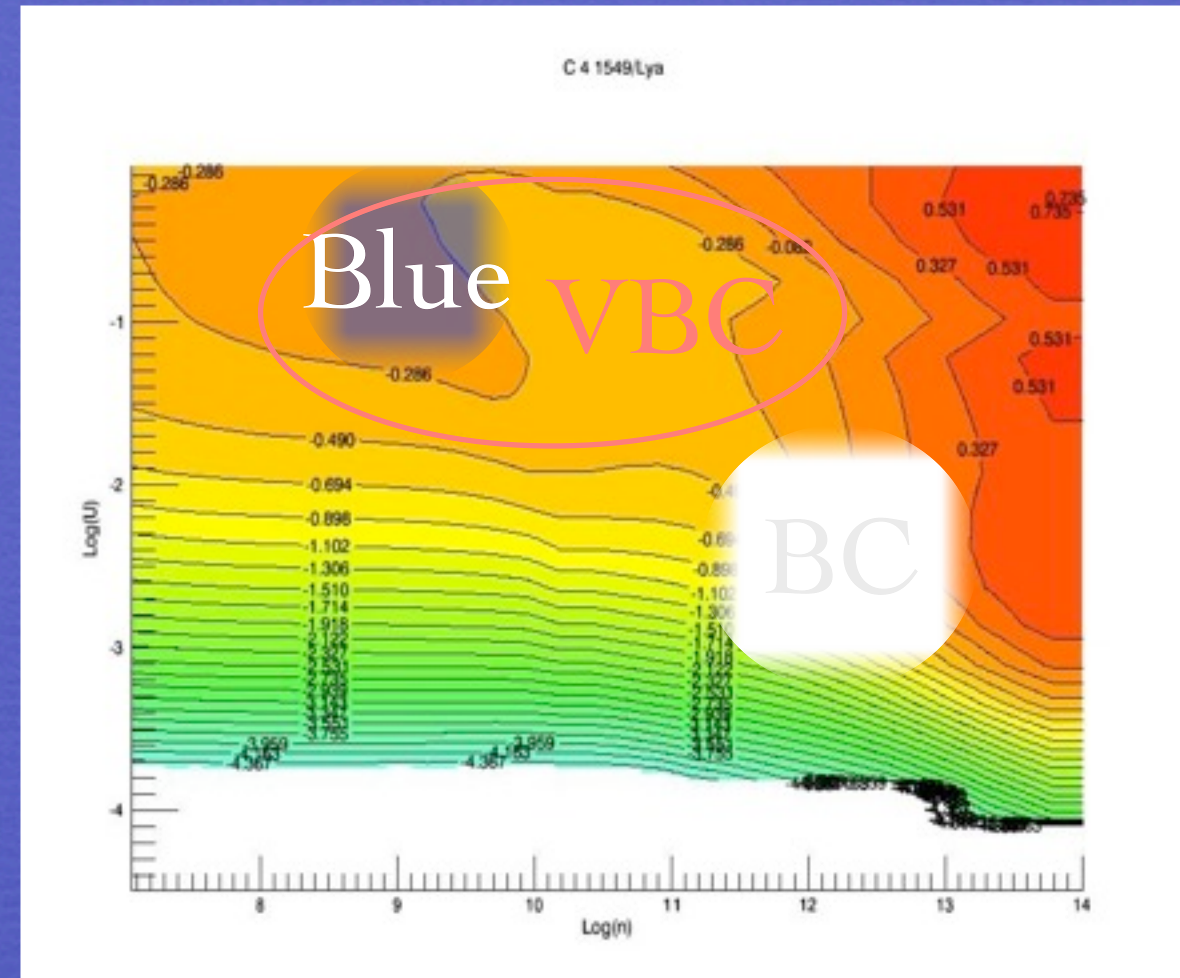
C 4 1549/Lya
Blue
VBC
BC
Log(U)
Log(n)

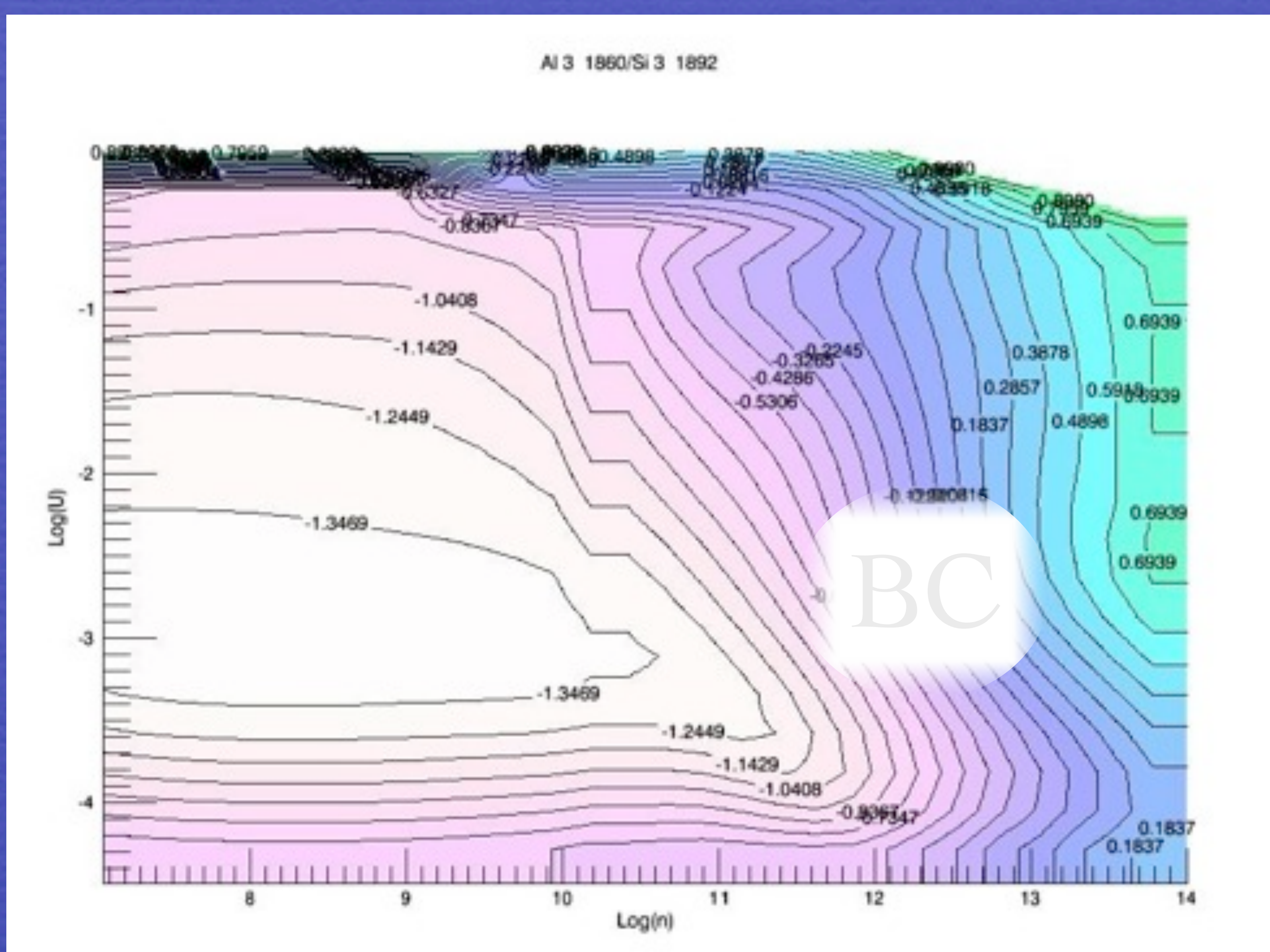
Al 3 1860/Si 3 1892
BC
Log(U)
Log(n)

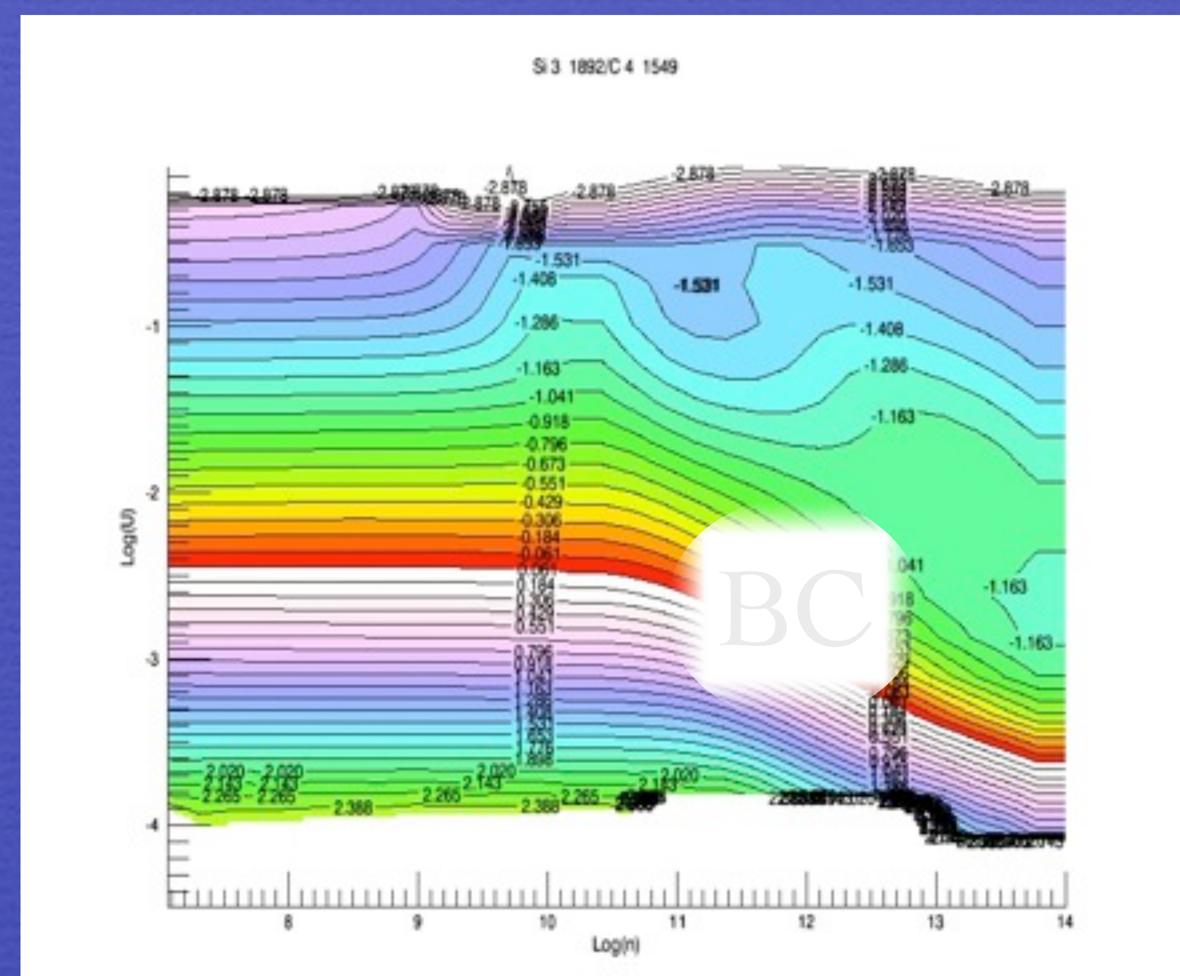
Si 3 1892/C 4 1549
BC
Log(U)
Log(n)

A microlensing study of the Einstein cross (QSO 2237+0305): CIV results

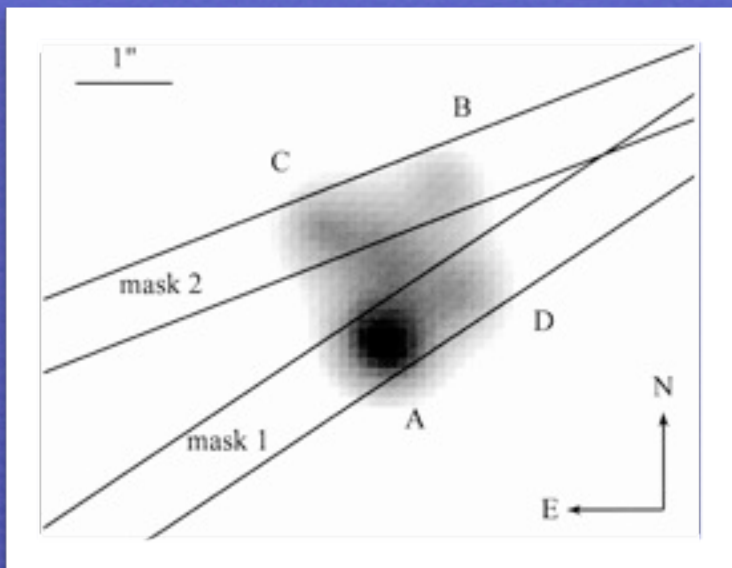

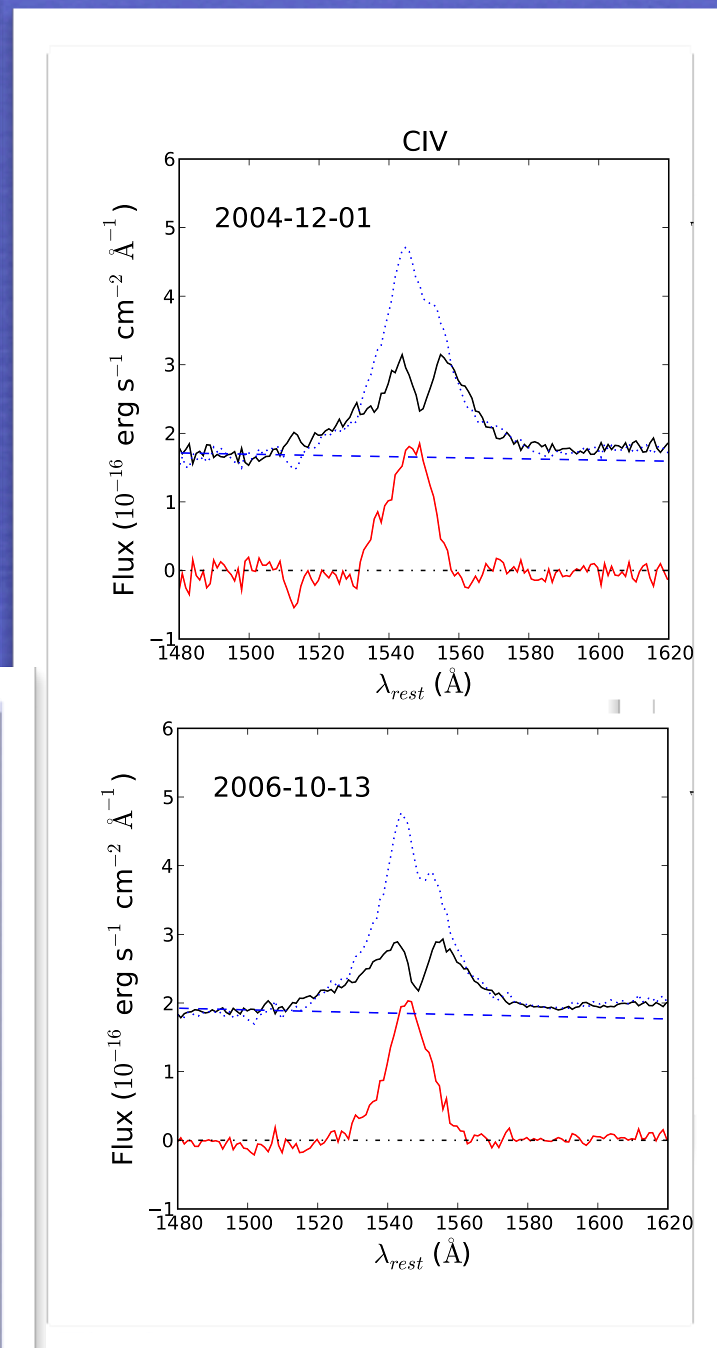

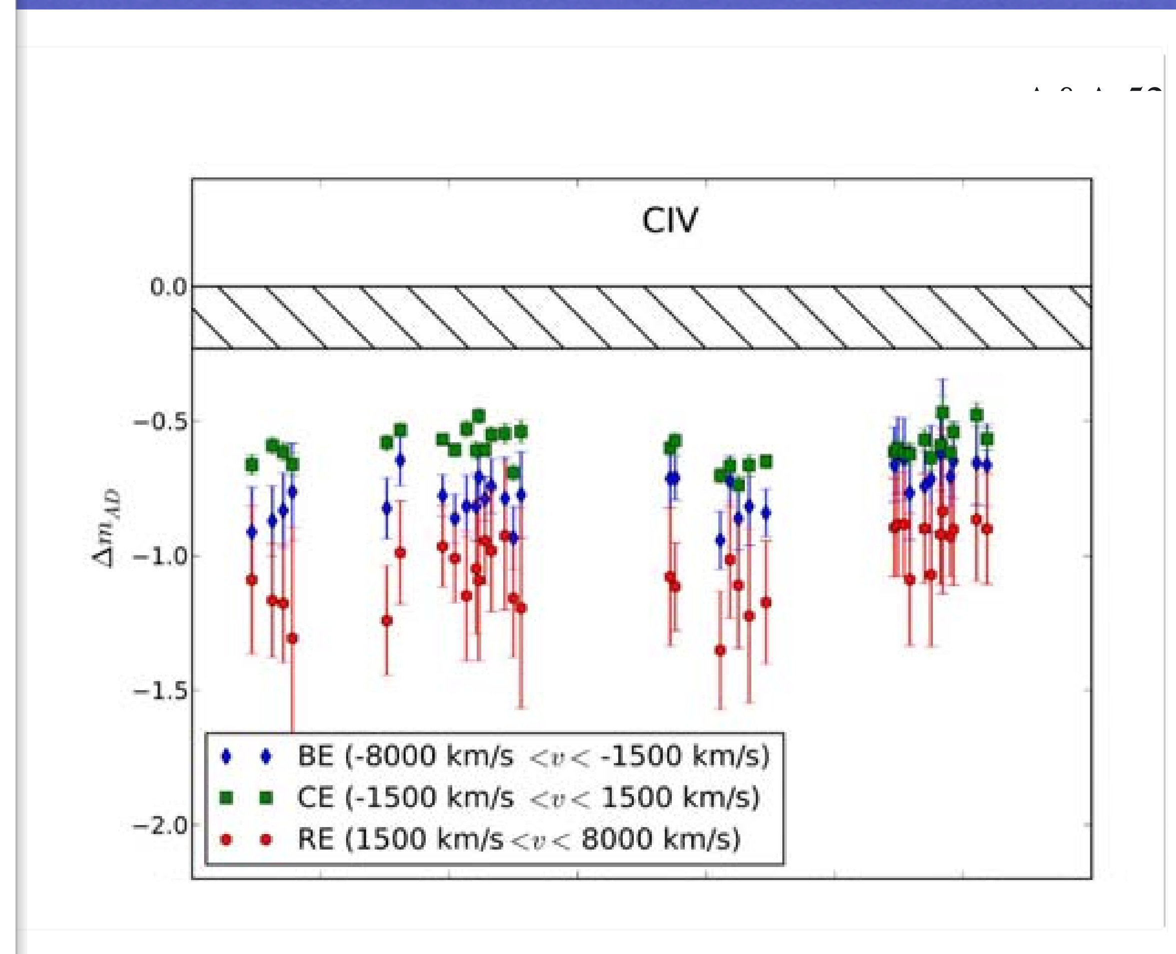

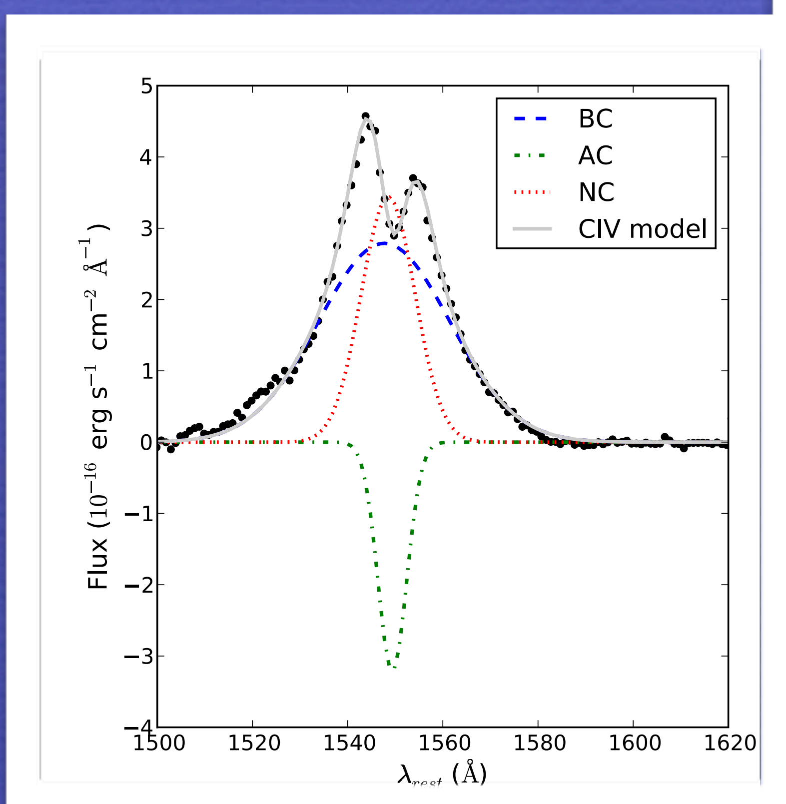

Eigenbrod et al. 2008; Sluse et al. 2011

POP A: HIL WIND (BLUESHIFTED COMPONENT)

moderate N_c, low density, high ionization

weaker in Pop. B and especially radio-loud sources

NON VIRIAL

POP B: VERY BROAD COMPONENT

high ionization, large N_c, large range of density

HIL, LIL stratified emitting region from BC to VBC

NON VIRIAL

Including non virial components:

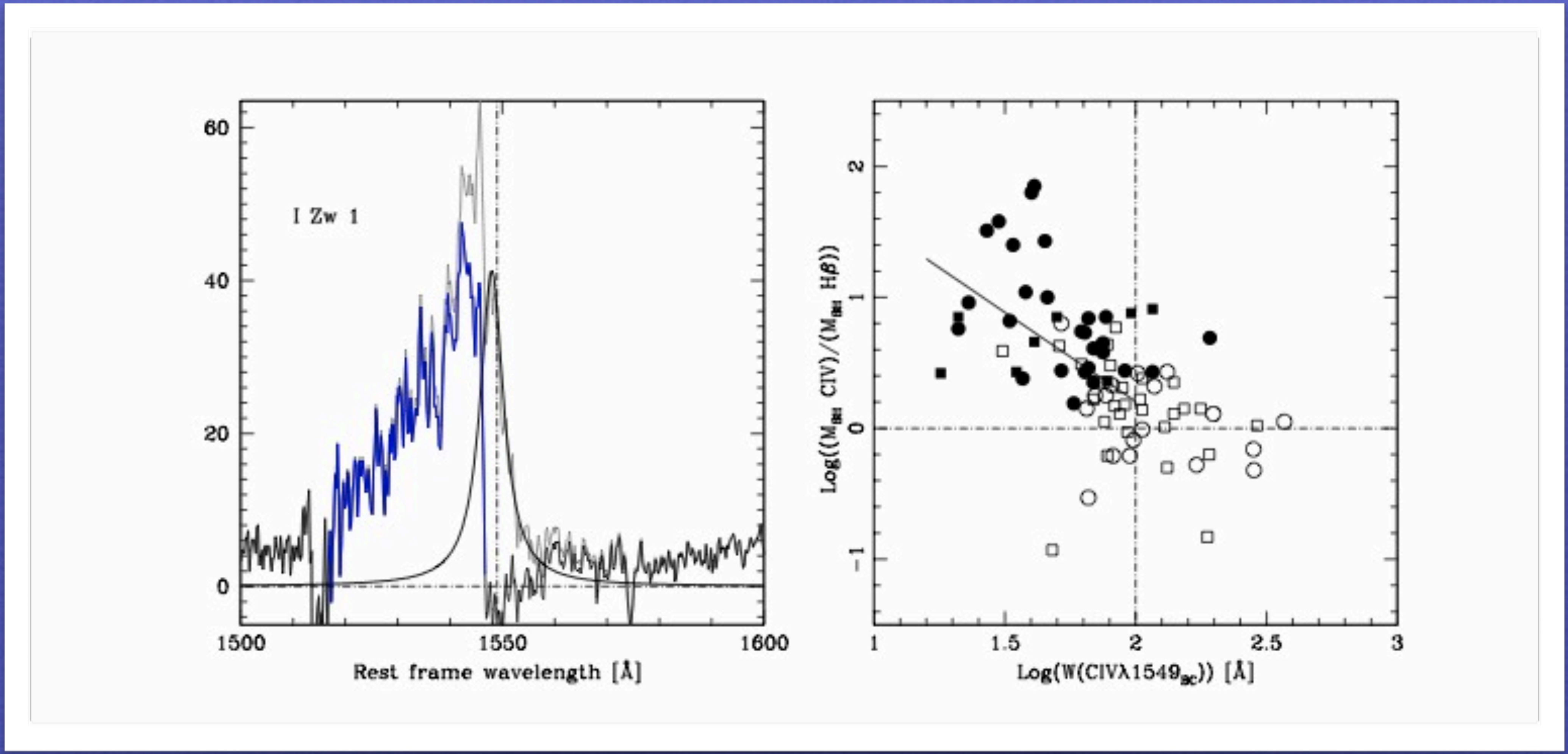

Sulentic et al. 2007

BROAD COMPONENT

emitting all LILs, low ionization, high density, large N_c

presumed VIRIAL component whose width can be used for M_{BH} computations

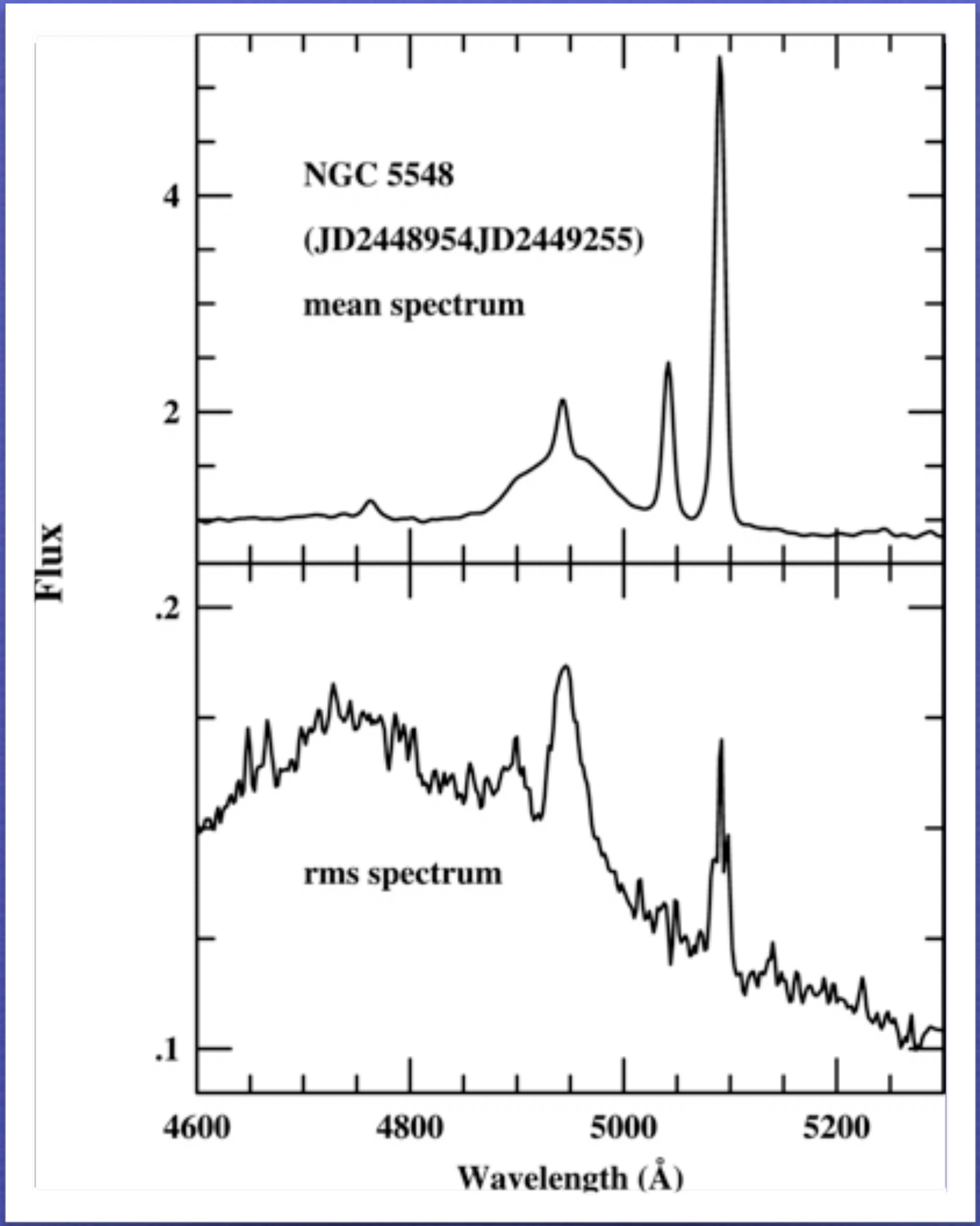

Peterson et al. 2004

Single epoch approximation to the reverberating part of the line

"Photoionization" mass computations

$$M_{\rm BH} = \frac{f r_{\rm BLR} ({\rm FWHM})^2}{G}$$

$$U = \frac{\int_{\nu_0}^{+\infty} \frac{L_\nu}{h\nu} d\nu}{4\pi r_{\rm BLR} n_{\rm e} c}$$

$$r_{\rm BLR} = \left(\frac{\int_{\nu_0}^{+\infty} \frac{L_\nu}{h\nu} d\nu}{4\pi U n_{\rm e} c} \right)^{\frac{1}{2}}$$

$$r_{\rm BLR} = \underbrace{\frac{1}{(4\pi c)^{\frac{1}{2}}}}_{\rm const.} \underbrace{(U n_{\rm e})^{-\frac{1}{2}}}_{\rm diagnostics} \left(\underbrace{\int_{\nu_0}^{+\infty} \frac{L_\nu}{h\nu} d\nu}_{\#\ \rm ionizing\ \ photons} \right)^{\frac{1}{2}}$$

Reverberation of Hβ

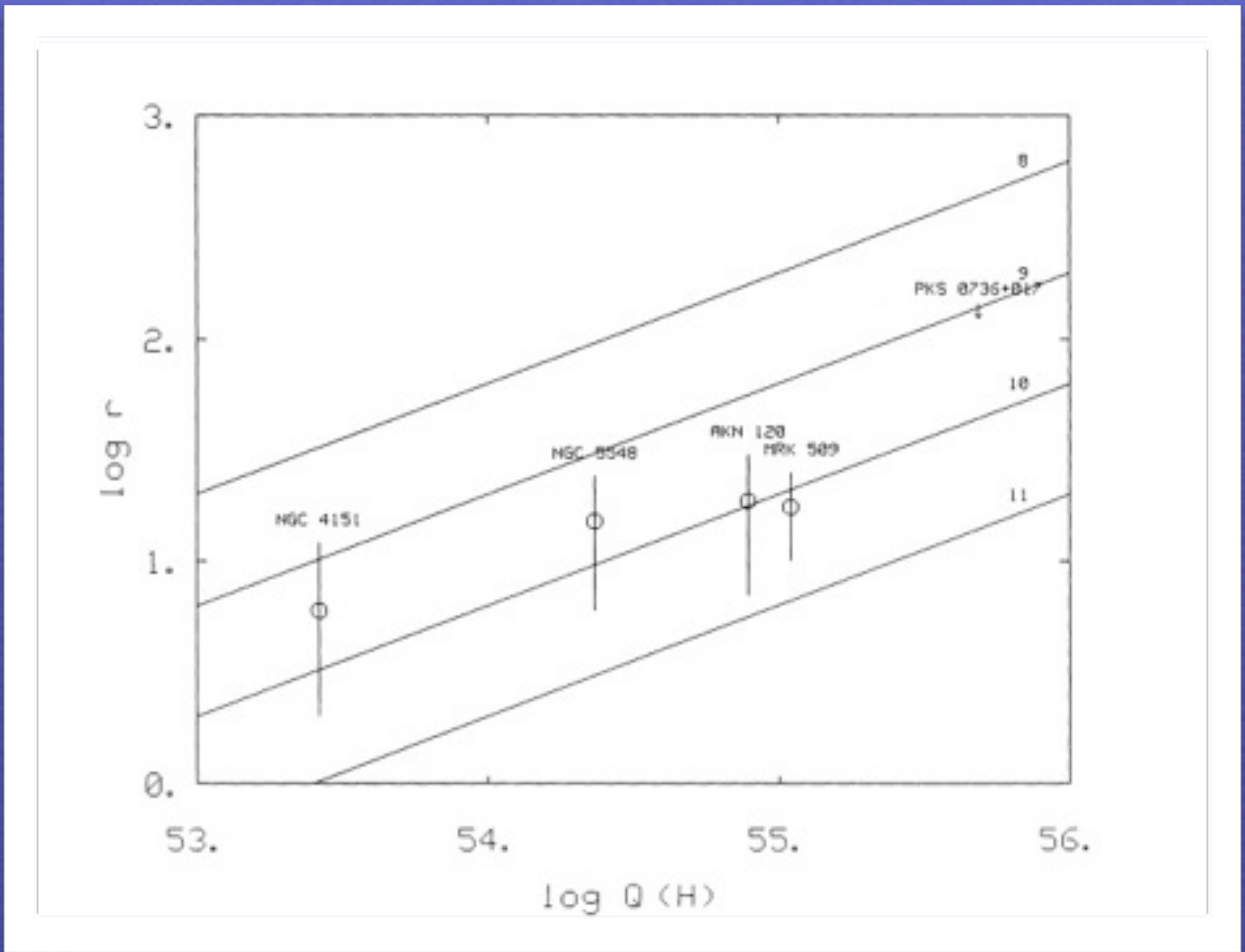

Padovani 1988

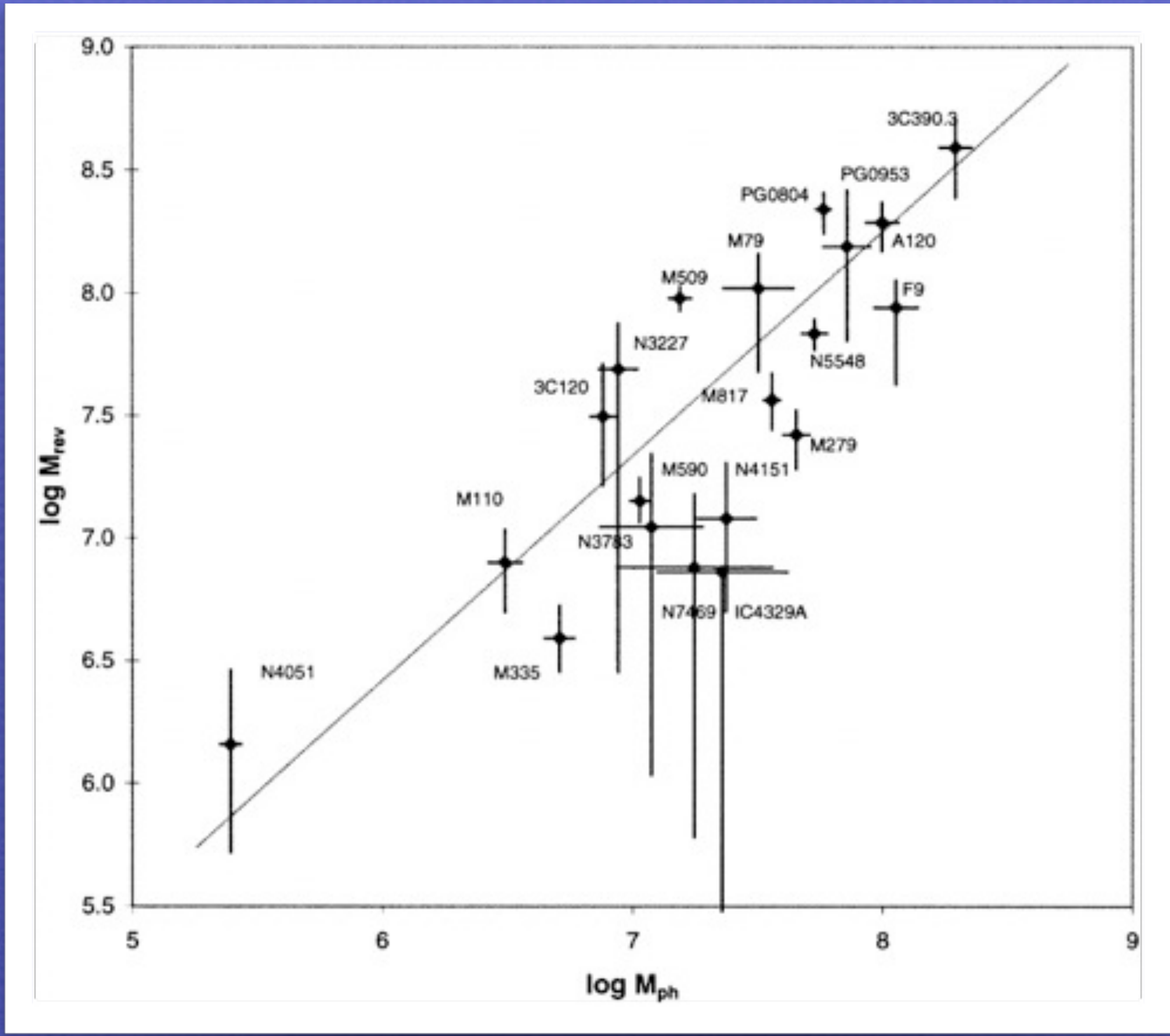

Wandel et al. 1999

$$(Un) \approx 10^{9.8}\mathrm{cm}^{-3}$$

Number of ionizing photons

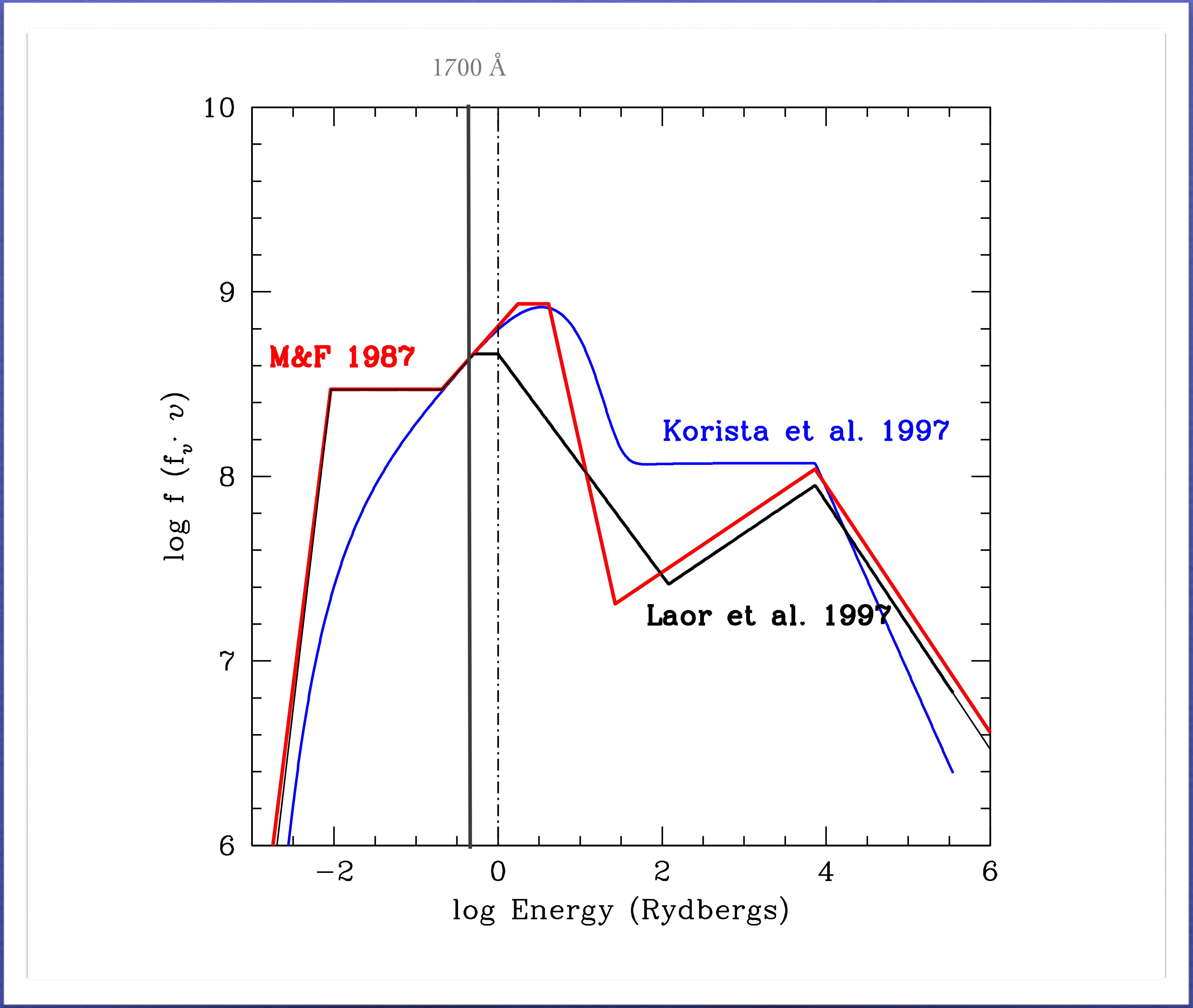

Same f_λ at 1700Å $\Rightarrow$ Q(H)(M&F)≈2Q(H)(L97)

Diagnostics from the rest-frame UV spectrum

TABLE 1
LINES IN THE 1350–2000 Å SPECTRAL RANGE

Ion	λ [Å]	X [eV]	$E_l - E_u$ [eV]	Transition	A_{ki} [s^{-1}]	n_c [cm^{-3}]	Note
Si IV	1393.755	45.20	0.000 - 8.896	$^2P^o_{3/2} \rightarrow {}^2S_{1/2}$	$8.80 \cdot 10^8$	···	1
Si IV	1402.770	45.20	0.000 - 8.839	$^2P^o_{1/2} \rightarrow {}^2S_{1/2}$	$8.63 \cdot 10^8$	···	1
C IV	1548.202	47.89	0.000 - 8.008	$^2P^o_{3/2} \rightarrow {}^2S_{1/2}$	$2.65 \cdot 10^8$	···	1
C IV	1550.774	47.89	0.000 - 7.995	$^2P^o_{1/2} \rightarrow {}^2S_{1/2}$	$2.64 \cdot 10^8$	···	1
Si II	1808.00	8.15	0.000 - 6.857	$^2D^o_{3/2} \rightarrow {}^2P_{1/2}$	$2.54 \cdot 10^6$	···	1
Si II	1816.92	8.15	0.036 - 6.859	$^2D^o_{5/2} \rightarrow {}^2P_{3/2}$	$2.65 \cdot 10^6$	···	1
Al III	1854.716	18.83	0.000 - 6.685	$^2P^o_{3/2} \rightarrow {}^2S_{1/2}$	$5.40 \cdot 10^8$	···	1
Al III	1862.790	18.83	0.000 - 6.656	$^2P^o_{1/2} \rightarrow {}^2S_{1/2}$	$5.33 \cdot 10^8$	···	1
[Si III]	1882.7	16.34	0.000 - 6.585	$^3P^o_2 \rightarrow {}^1S_0$	0.012	$6.4 \cdot 10^4$	1,2,3
Si III]	1892.03	16.34	0.000 - 6.553	$^3P^o_1 \rightarrow {}^1S_0$	16700	$2.1 \cdot 10^{11}$	1,4,5
[C III]	1906.7	24.38	0.000 - 6.502	$^3P^o_2 \rightarrow {}^1S_0$	0.0052	$7.7 \cdot 10^4$	1,2,6
C III]	1908.734	24.38	0.000 - 6.495	$^3P^o_1 \rightarrow {}^1S_0$	114	$1.4 \cdot 10^{10}$	1,2,4,5
Fe III	1914.066	16.18	3.727 - 10.200	$z^7P^o_3 \rightarrow a^7S_3$	$6.6 \cdot 10^8$	···	7

NOTE. — All wavelengths are in vacuum. (1) Ralchenko, Yu., Kramida, A.E., Reader, J., and NIST ASD Team (2008). NIST Atomic Spectra Database (version 3.1.5). Available at: http://physics.nist.gov/asd3. 2: Feibelman & Aller (1987). 3: n_c computed following Shaw & Dufour (1995). 4: Morton (1991). 5: Feldman (1992). 6: Zheng (1988). 7: Wavelength and A_{ki} from Ekberg (1993), energy levels from Edlén and Swings (1942).

CIV (Al III, Si IV)

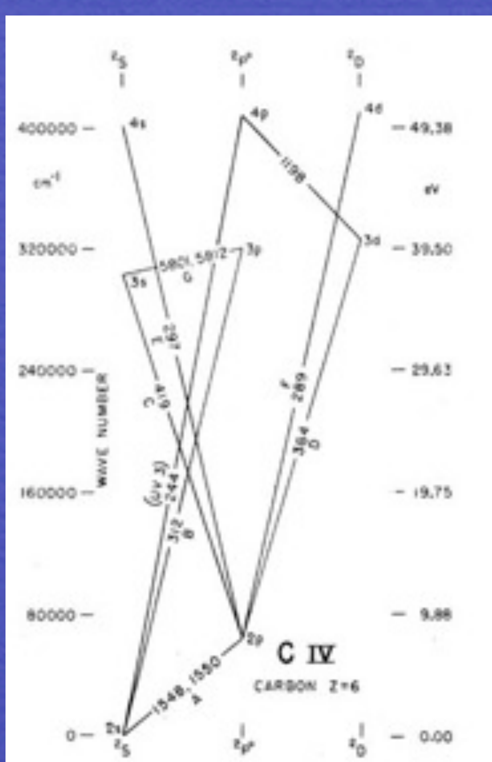

C III] (Si III])

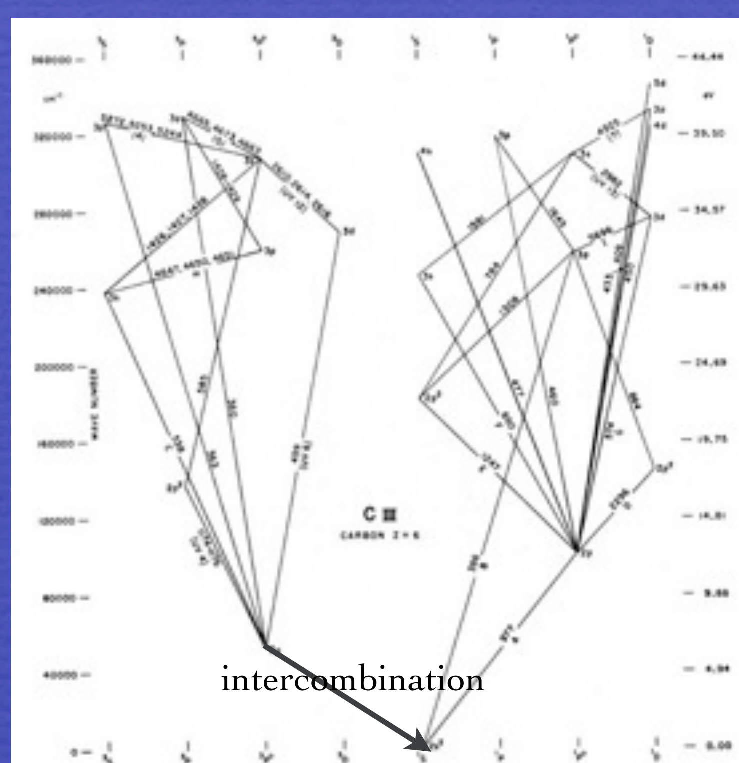

Si II

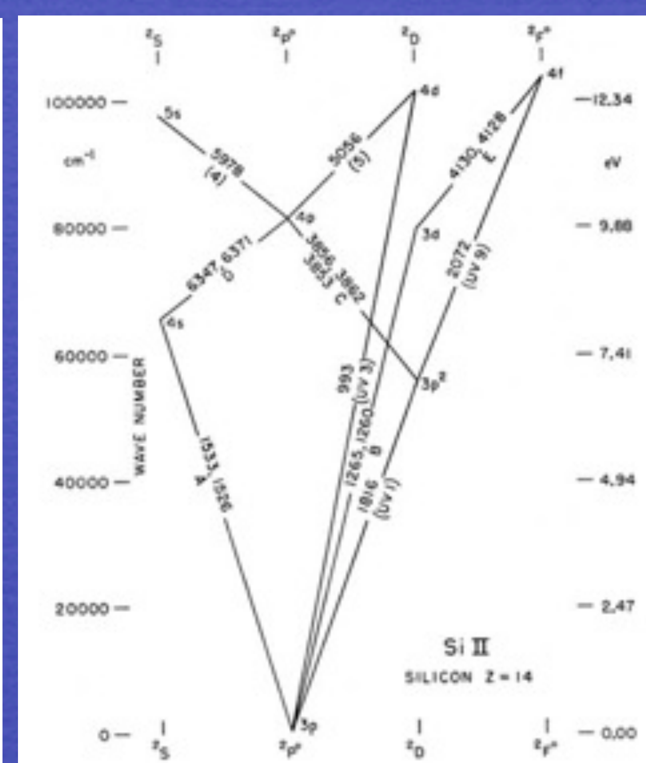

Fe III λ 1914, Lyα pumping

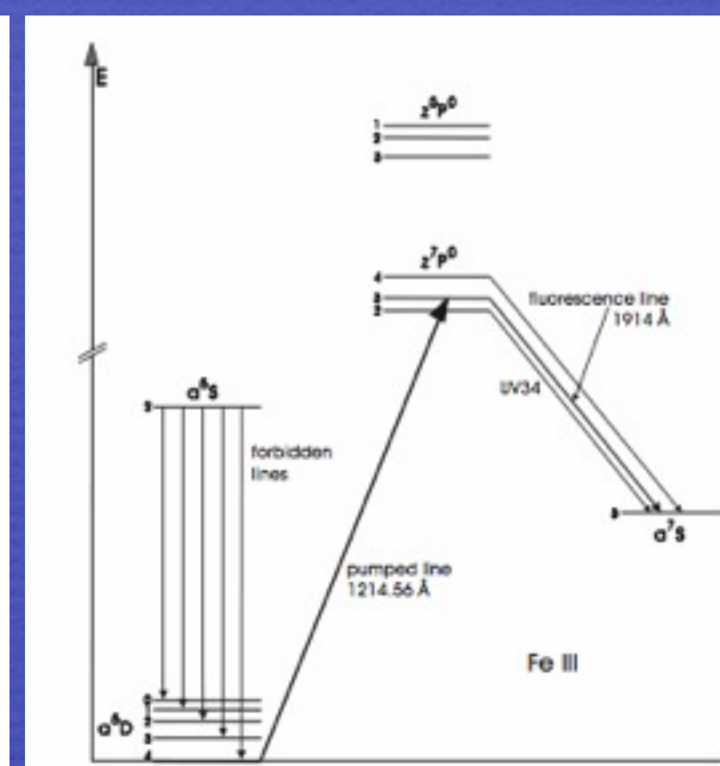

Ionization structure of the emitting gas slab

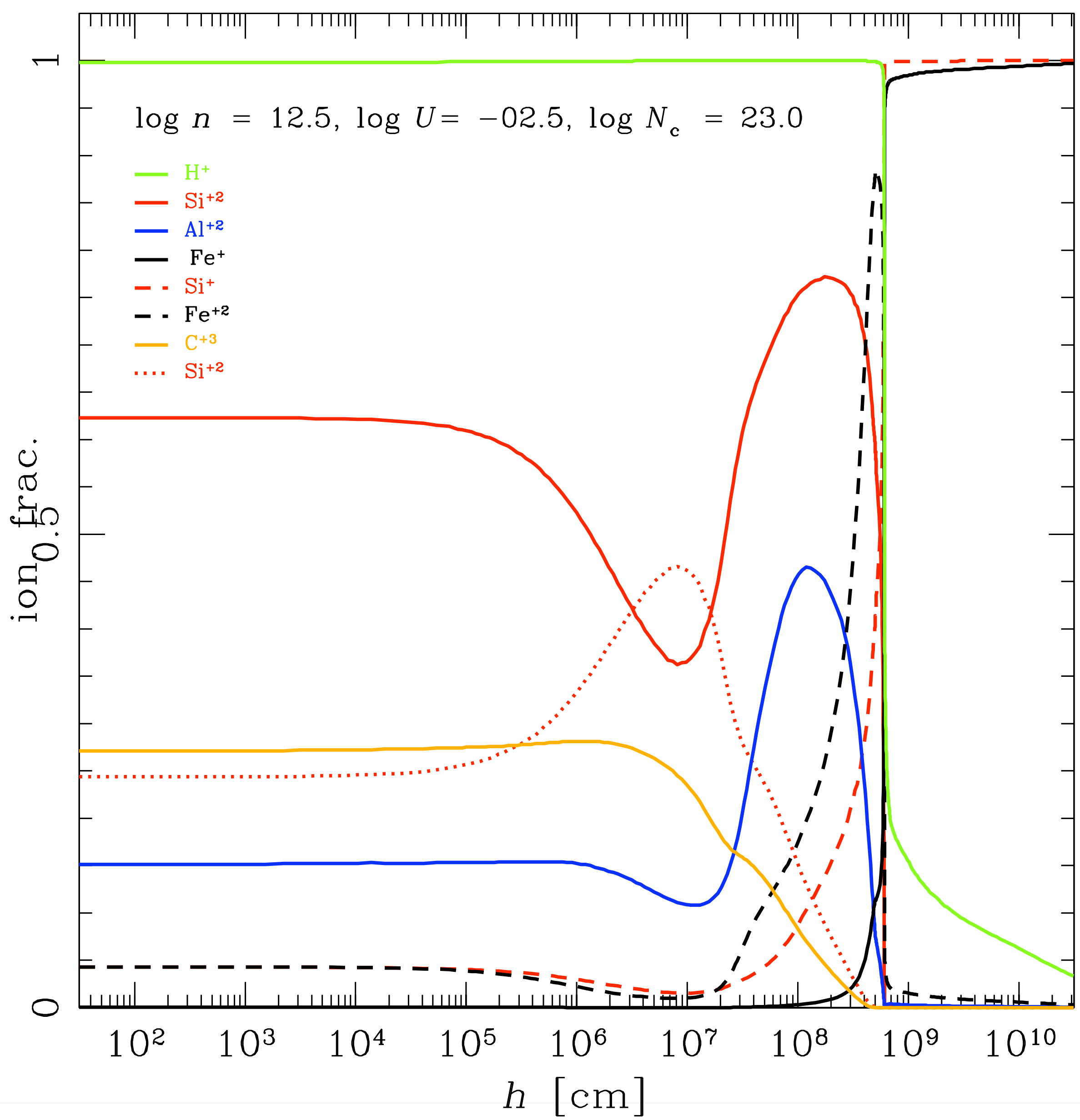

Line emissivity as a function of depth within the slab

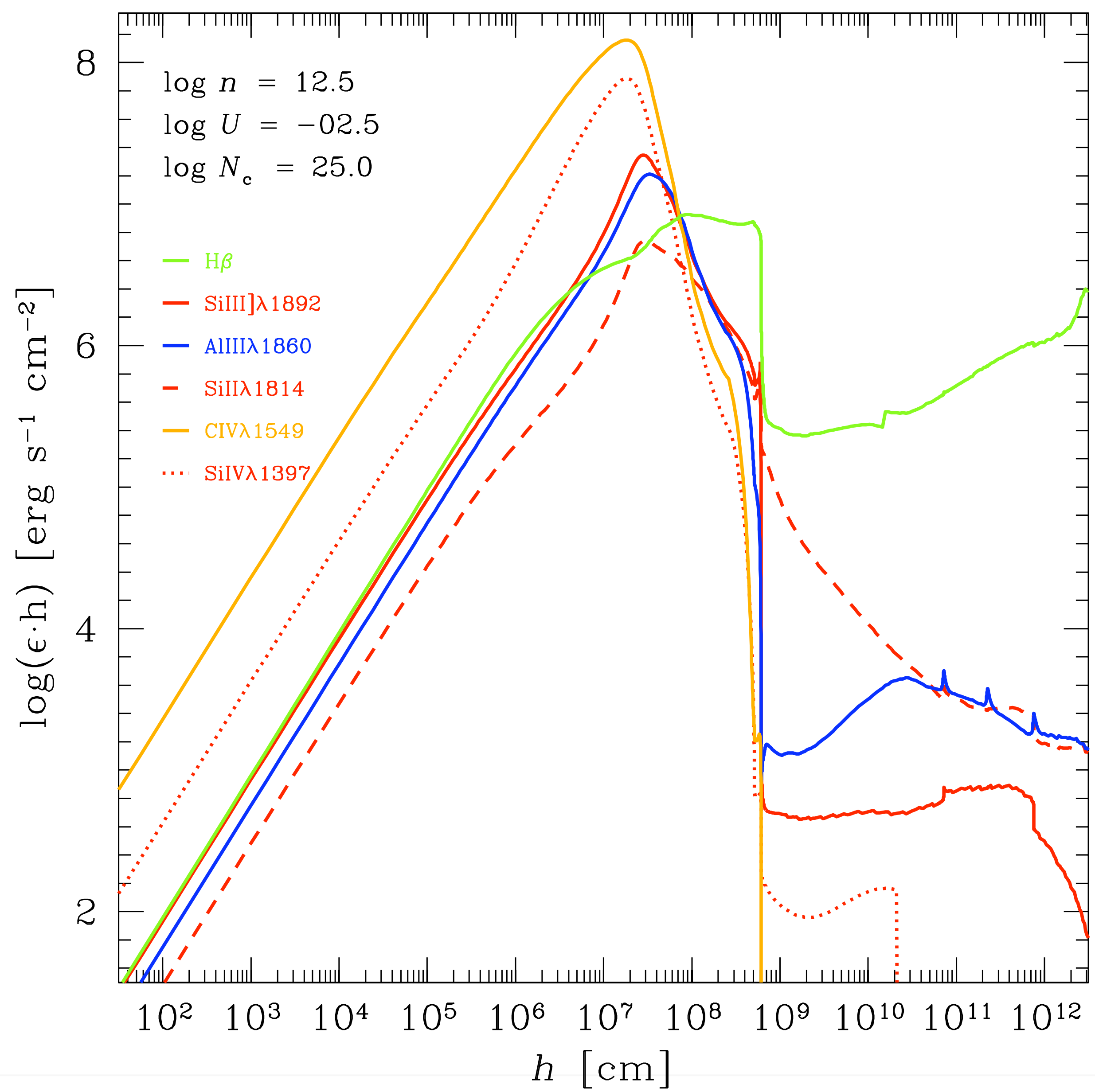

Diagnostic Intensity Ratios

S IV λ1397/Si III] λ1892 Si II 1814/Si III] λ1892	*independent on metallicity* *sensitive to ionization*
C IV λ1549/Si IV] λ1397	*sensitive to metallicity*
Al III λ1860/Si III] λ1892	*sensitive to density*
C IV λ1549/Al III λ1860 C IV λ1549/Si III] λ1892	*sensitive to ionization* *dependent on metallicity*

Measured with IRAF SPECFIT
along with continuum
Fe II, Fe III emission

The targets: high luminosity equivalents of NLSy1s

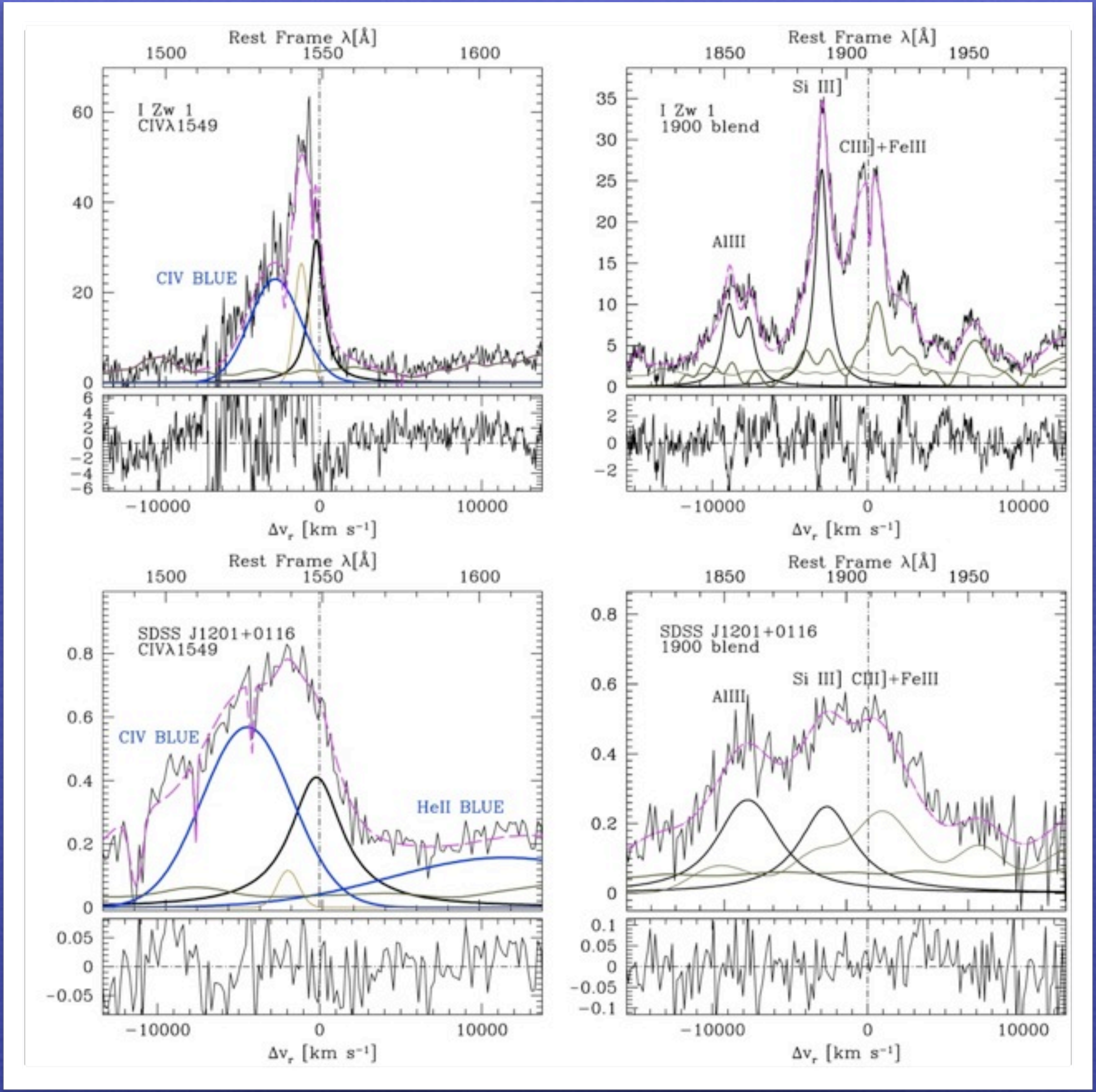

CLOUDY 08.00 photoionization computations

Ferland et al. 1998; cf Korista et al. 1997

19x29 array in logU x logn
metallicity solar, 5 Z⊙, 5 Z⊙ Si-Al enriched
Ferland & Mathews and Laor et. al. continua
Column density 10^{23} and 10^{25} cm^{-2}

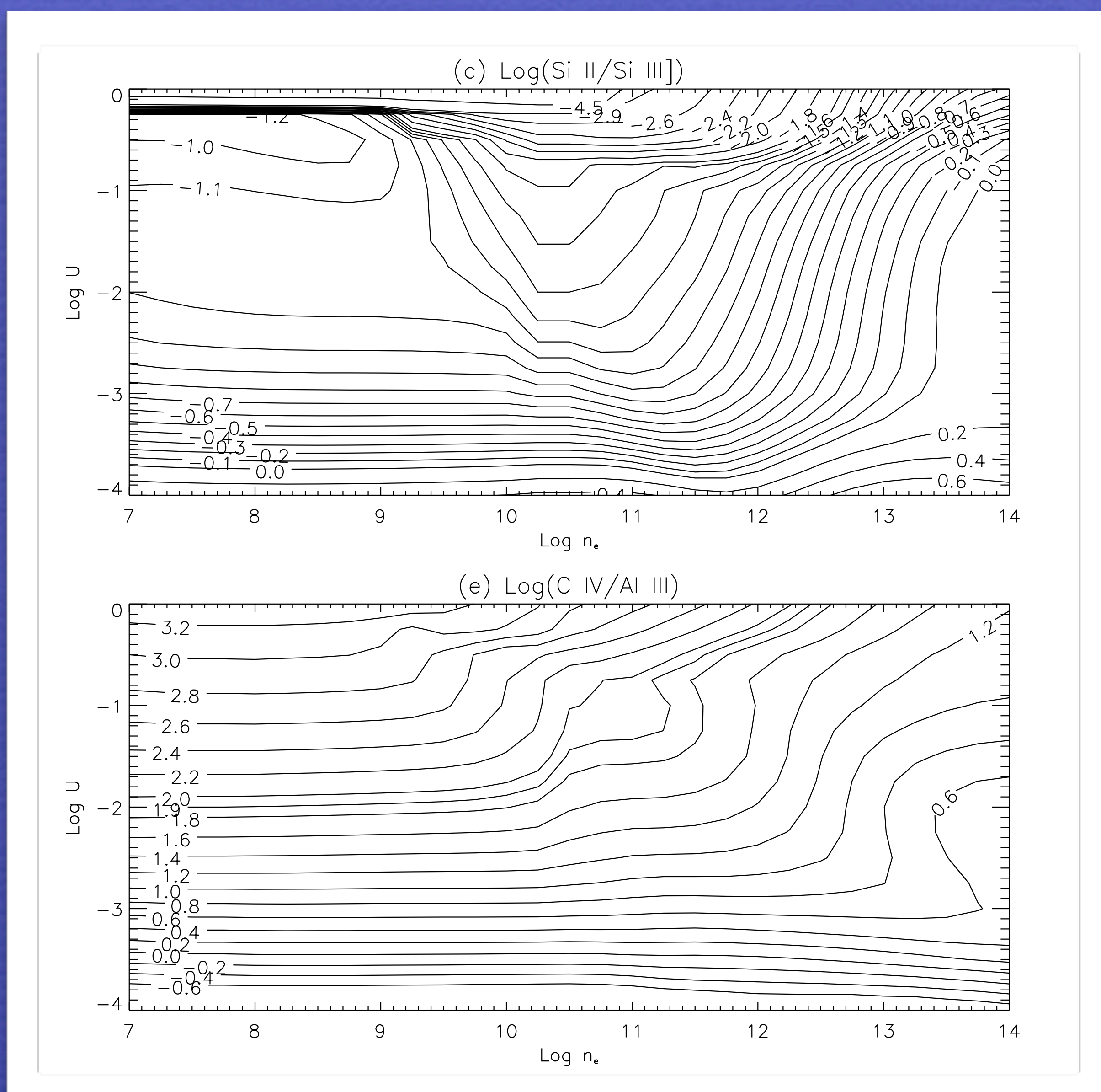

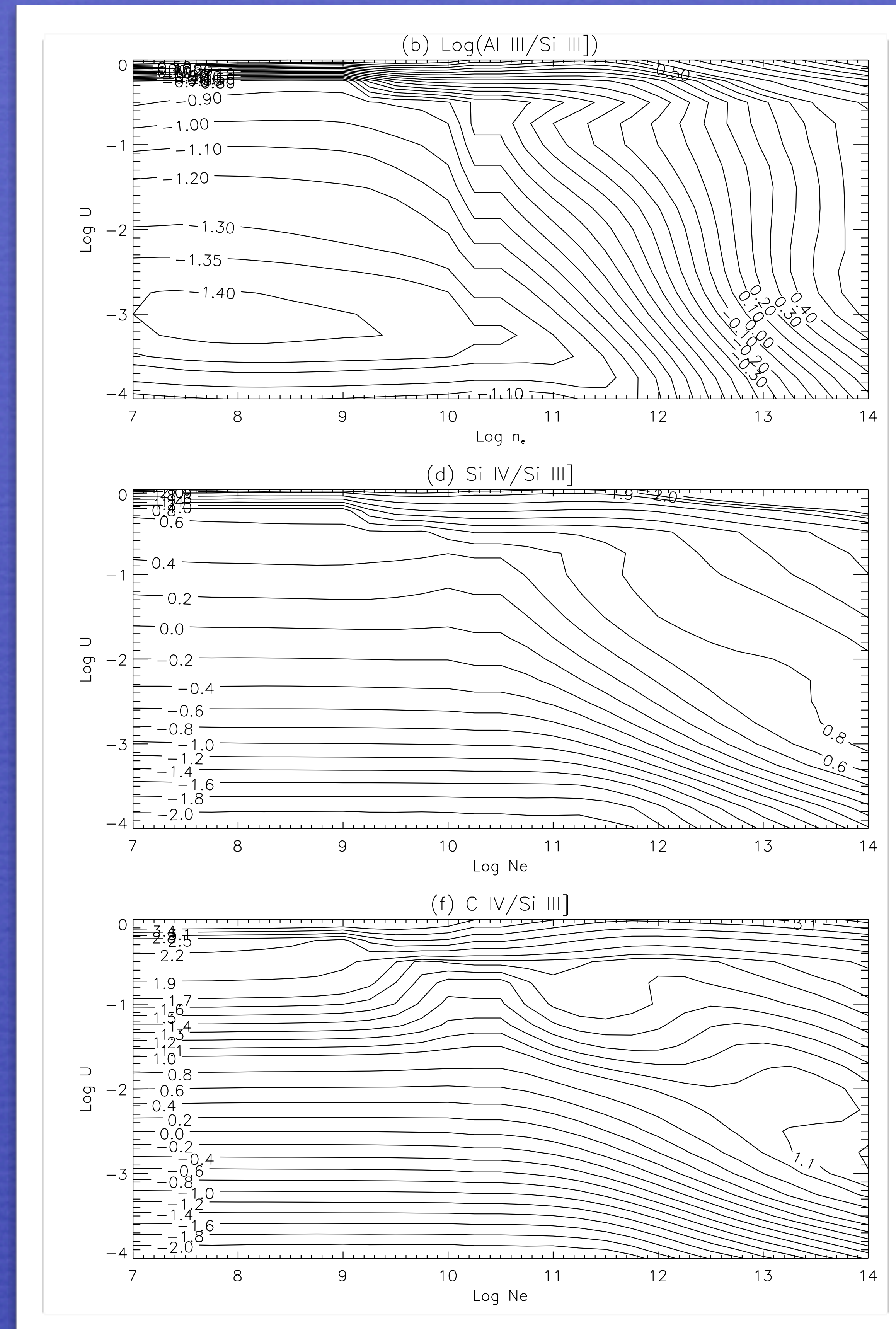

SDSS J1201+0116

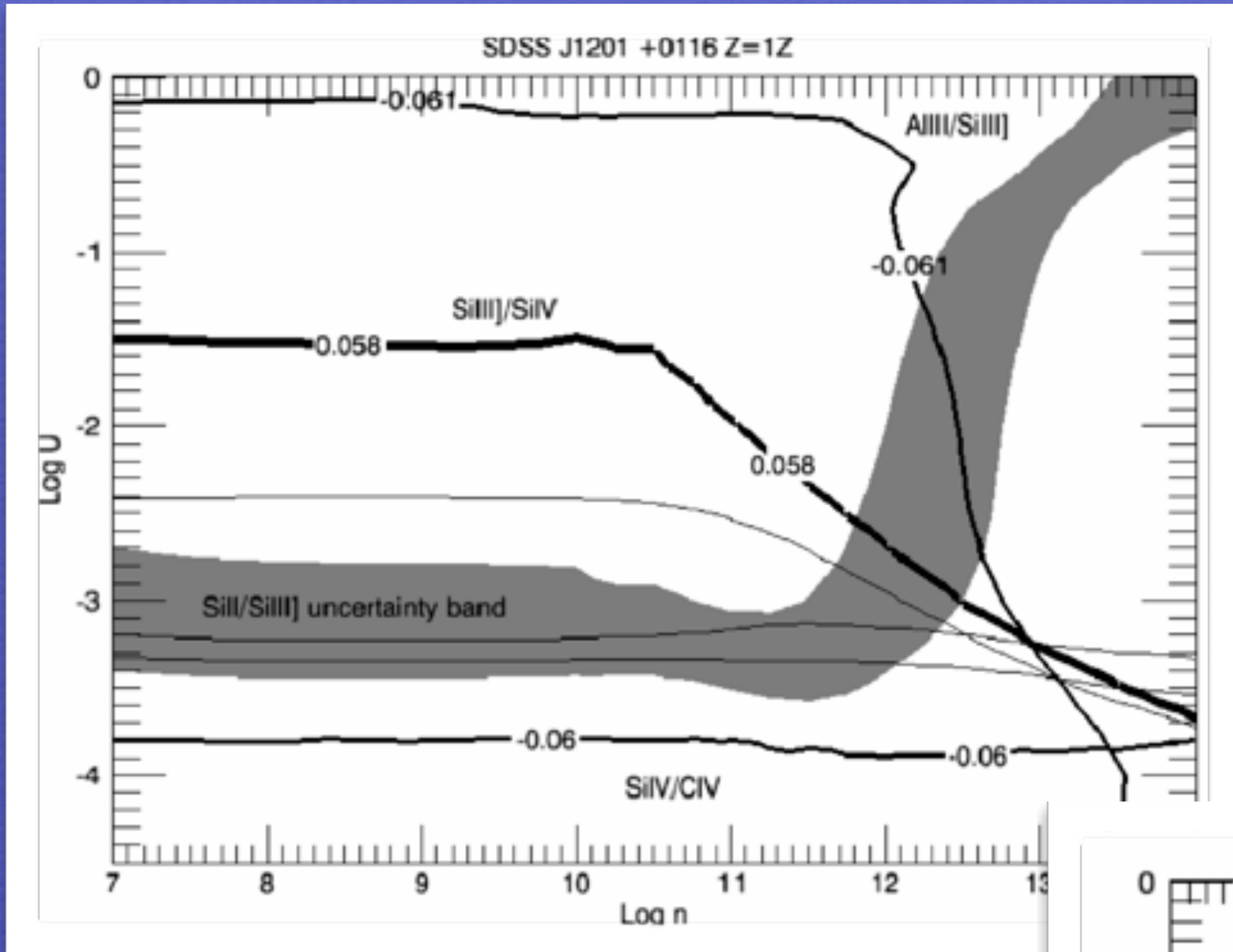

assumption of solar metallicity: unsatisfactory, unphysical

5 times solar metallicity with 3 times Si and Al enrichment: good convergence

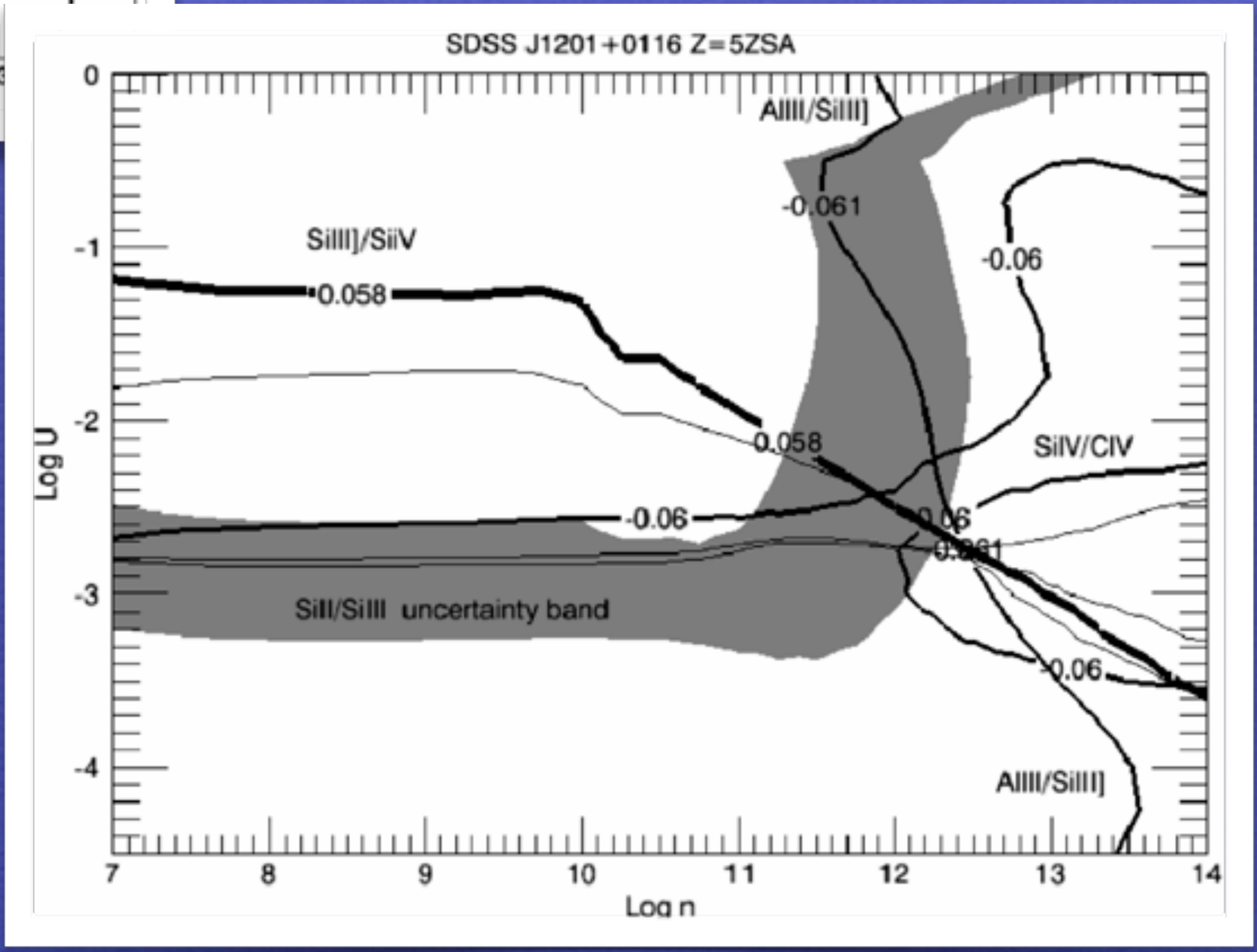

Sources of error

diagnostics: less than ±0.2 in log

$$r_{\rm BLR} = \underbrace{\frac{1}{(4\pi c)^{\frac{1}{2}}}}_{\rm const.} \underbrace{(Un_{\rm e})^{-\frac{1}{2}}}_{\rm diagnostics} \left(\underbrace{\int_{\nu_0}^{+\infty} \frac{L_\nu}{h\nu} d\nu}_{\#\ \rm ionizing\ \ photons} \right)^{\frac{1}{2}}$$

Δlog Q(H) ±0.065 [shape]

Δlog f_λ: ±0.08

$\Delta\log r_{\rm BLR} \approx 0.23$

$$M_{\rm BH} = \frac{f r_{\rm BLR} (\rm FWHM)^2}{G}$$

Δlog $f \approx$ not set

Δ log FWHM: ±0.16

$\Delta\log M_{\rm BH} \approx 0.3$ (2σ confidence)

Can the method be applied to the general population of quasars?

CIII] and VBC (Pop. B) complicate the issue but do not make it hopeless

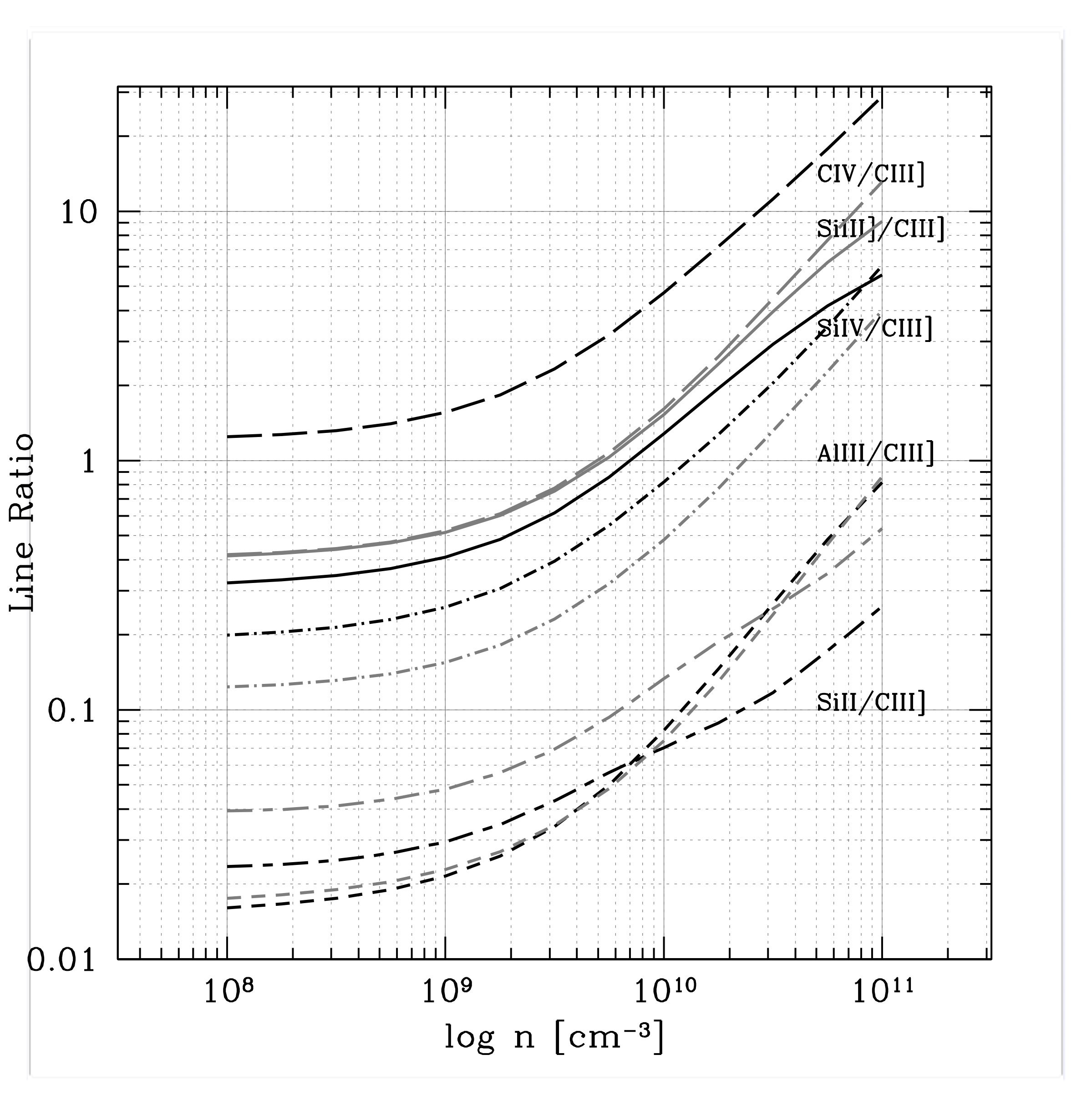

logΓ=-2; logΓ=-5

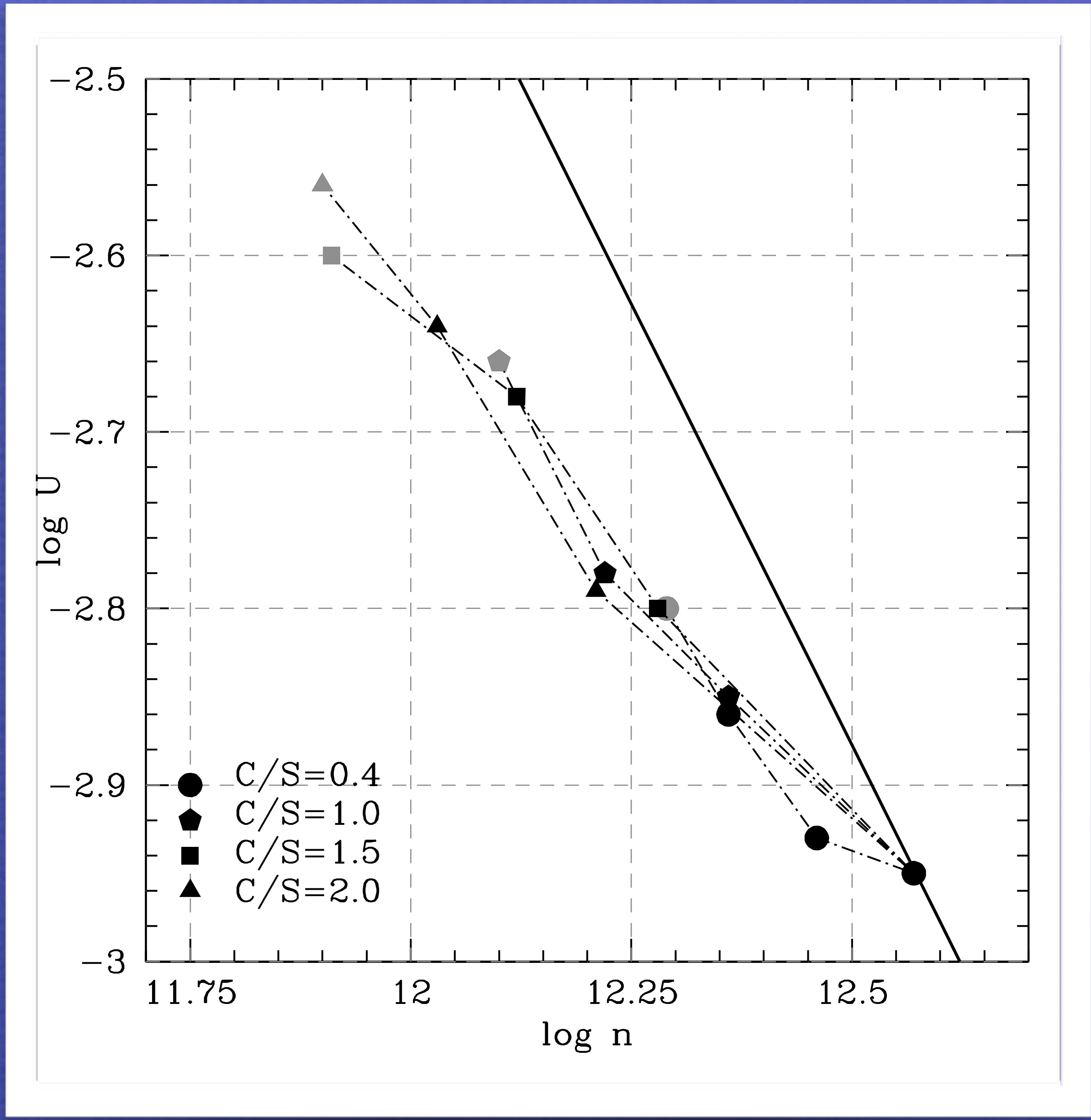

assumes logΓ=-2

Reverberation-mapped objects

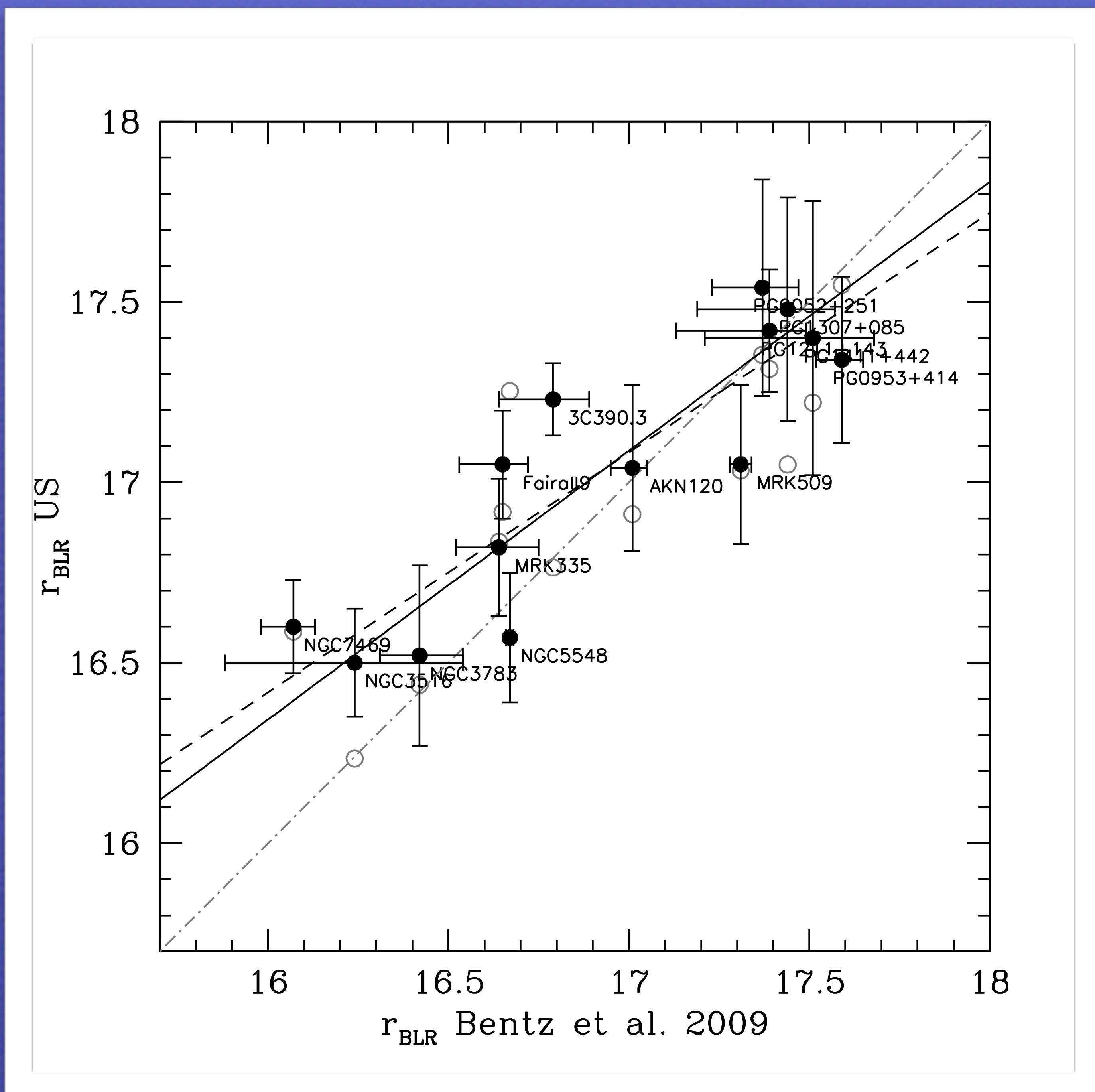

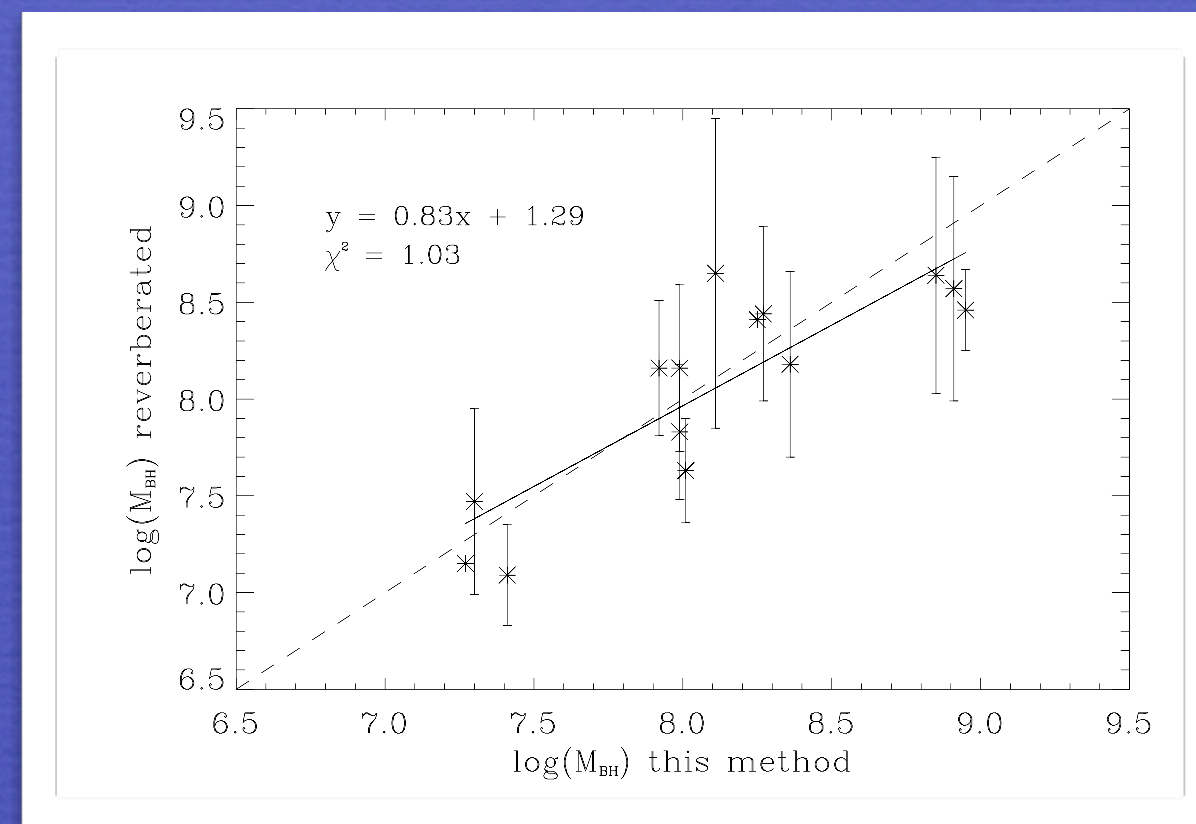

Negrete et al., in preparation

Toward higher redshift …

ESO
VLT

FORS

Pilot observations with FORS

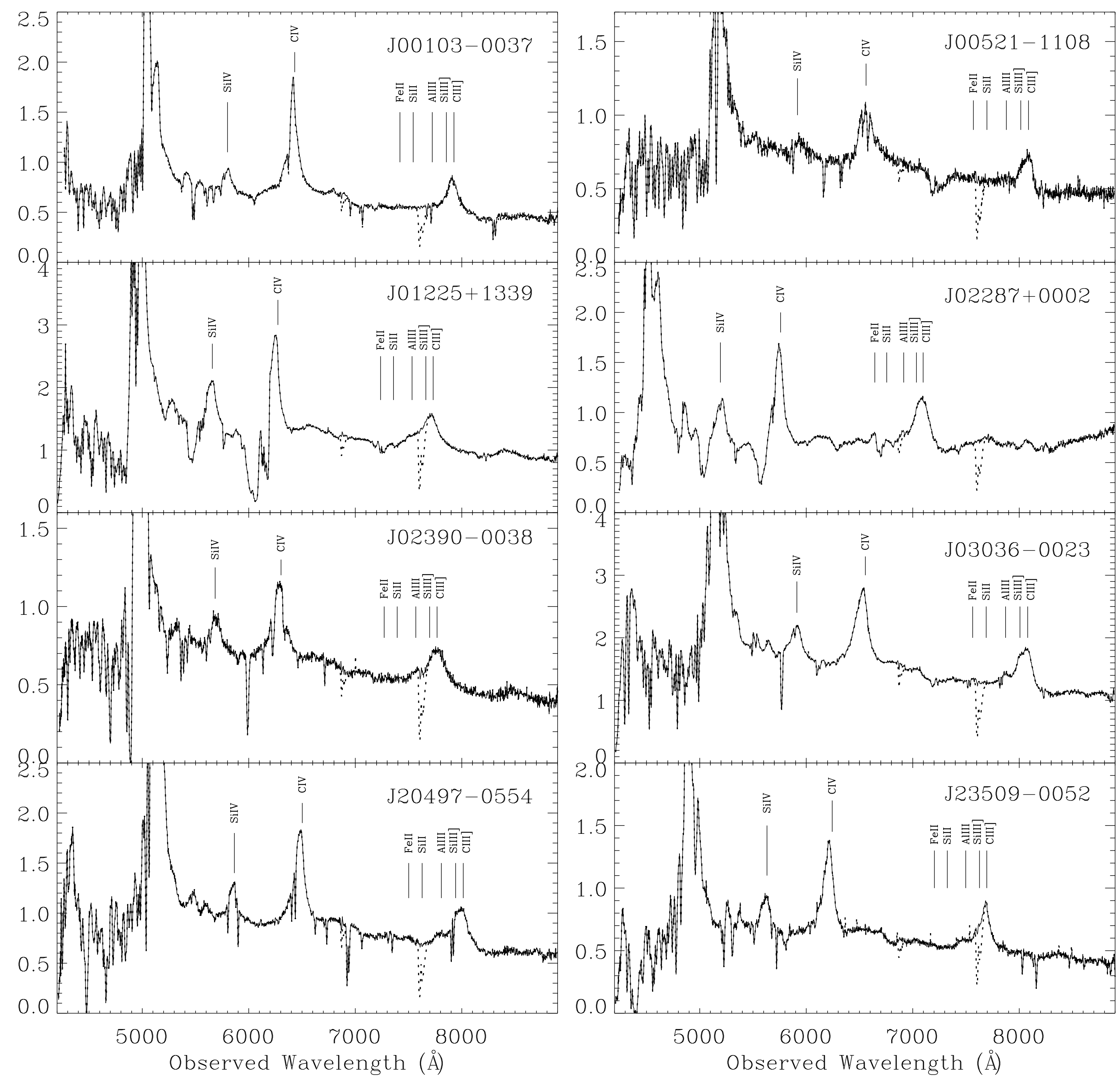

J03036-0023

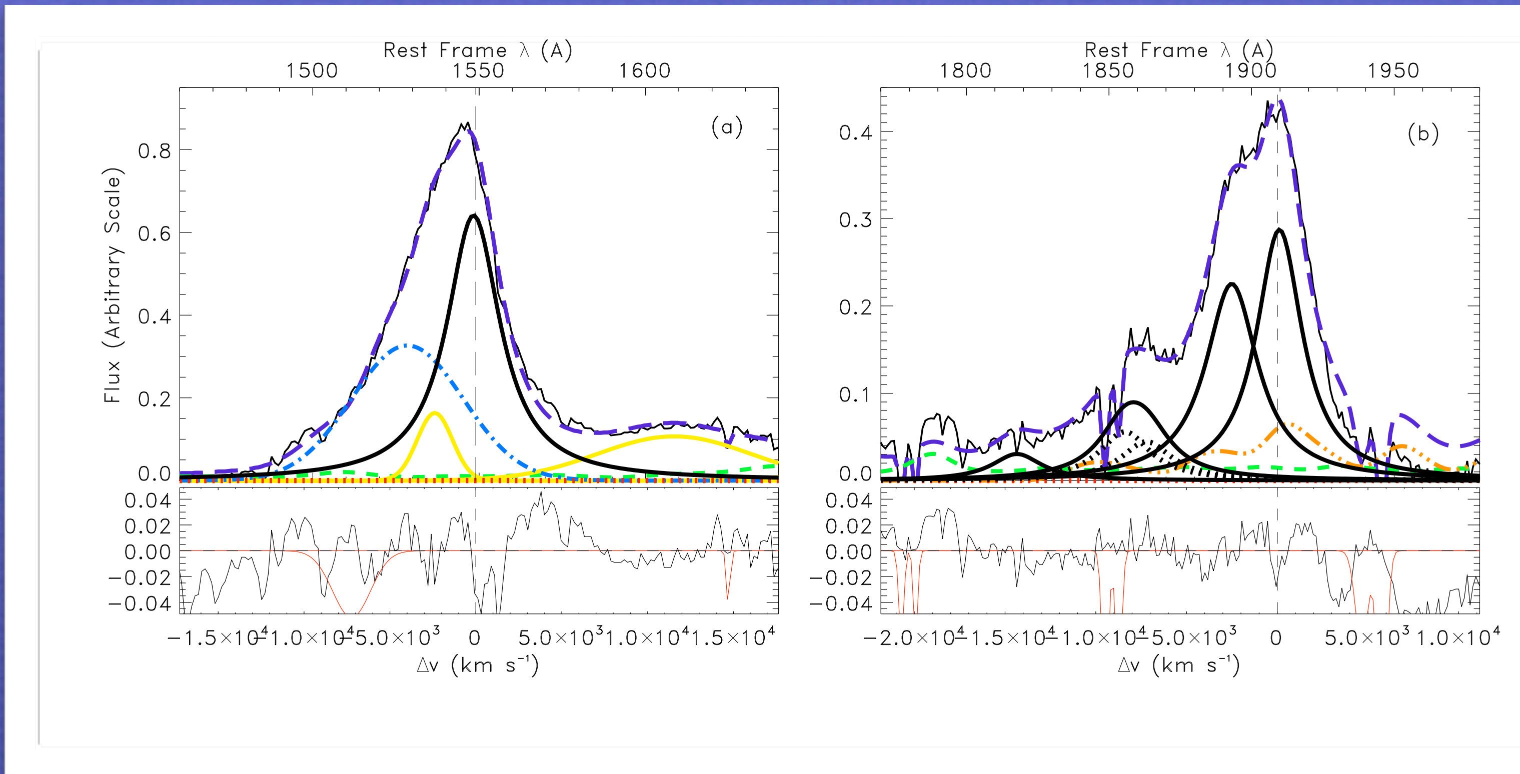

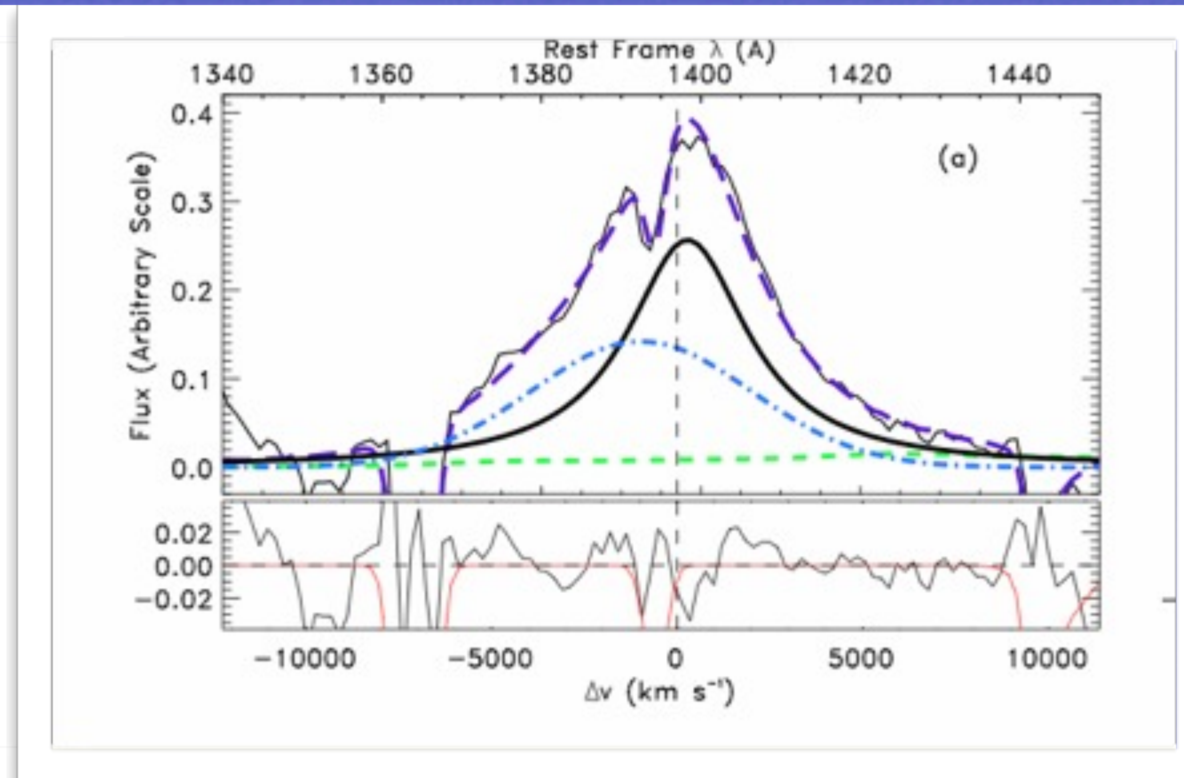

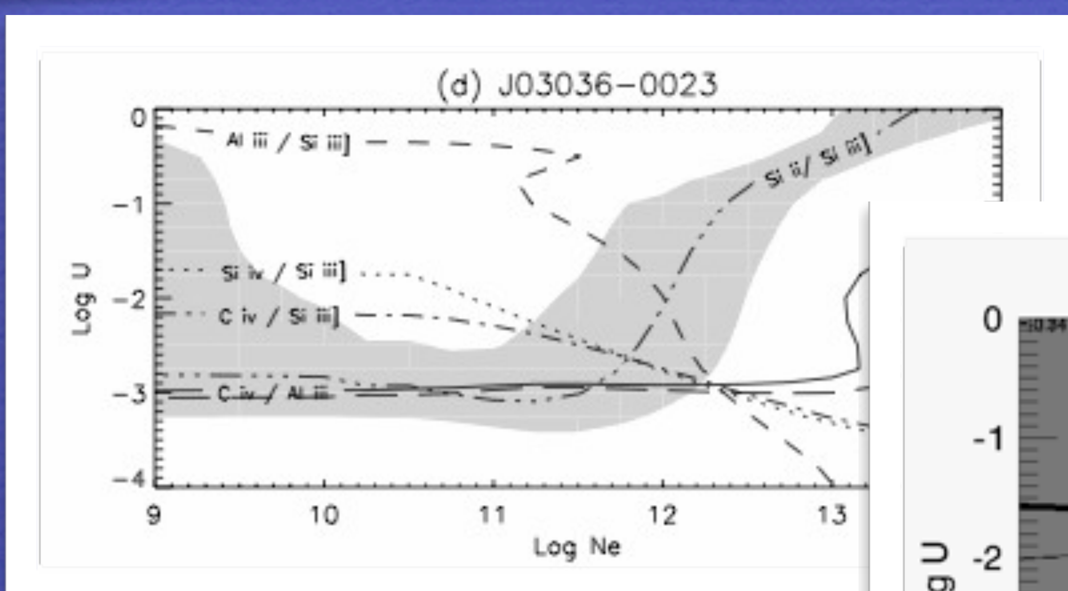

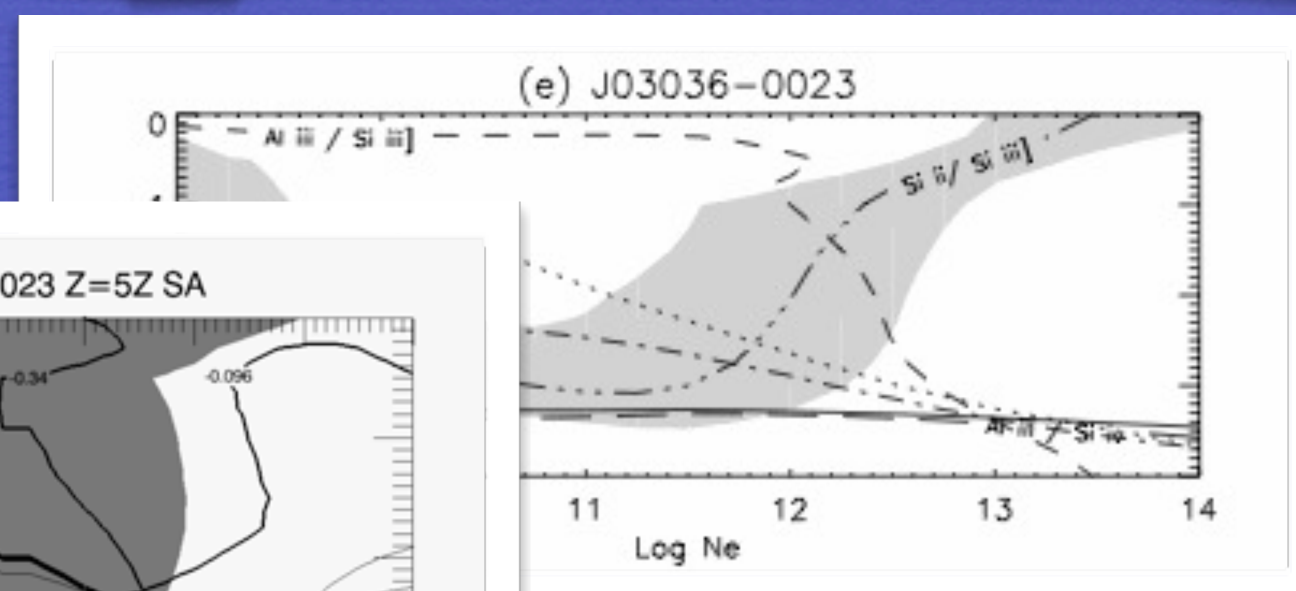

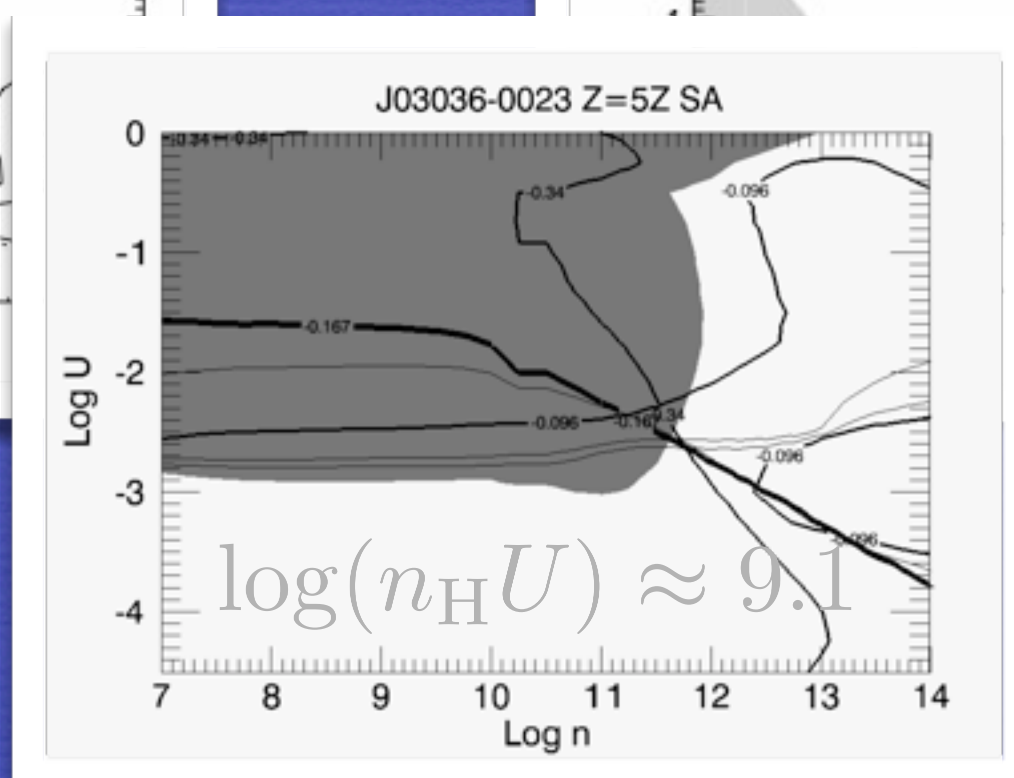

$$\log(n_{\mathrm{H}}U) \approx 9.4$$

$$\log(n_{\mathrm{H}}U) \approx 9.1$$

J00521-1108

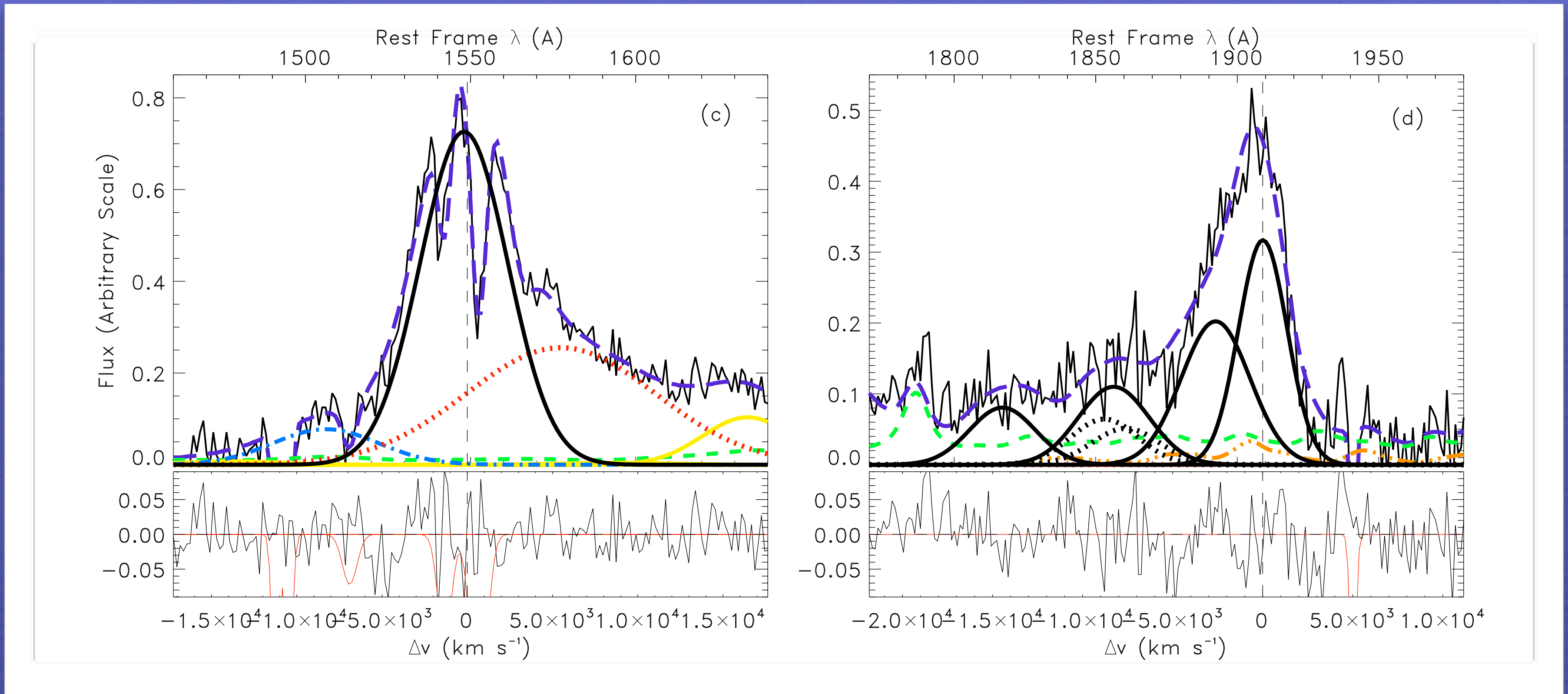

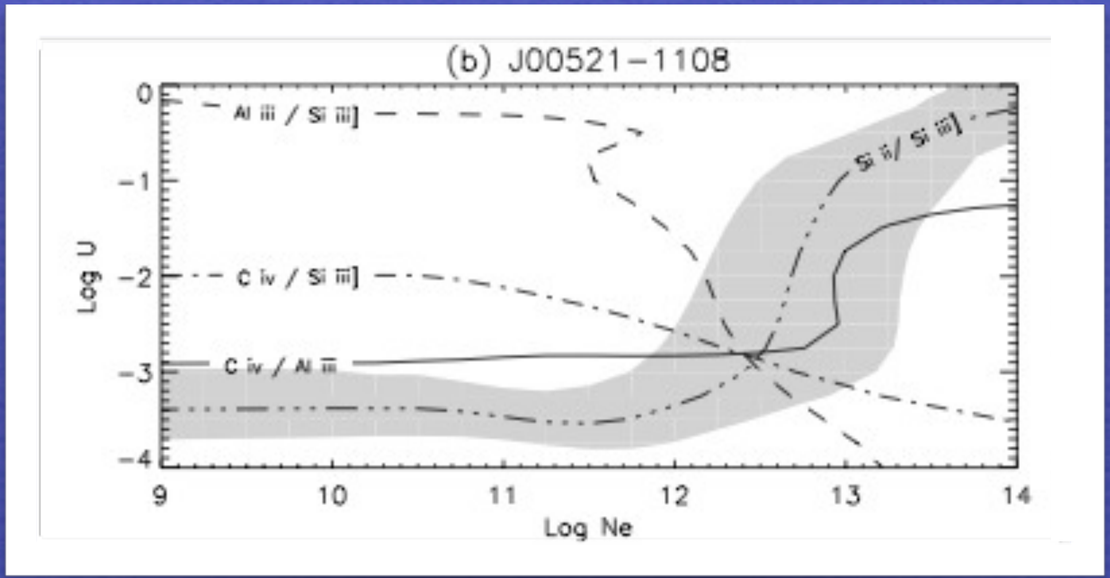

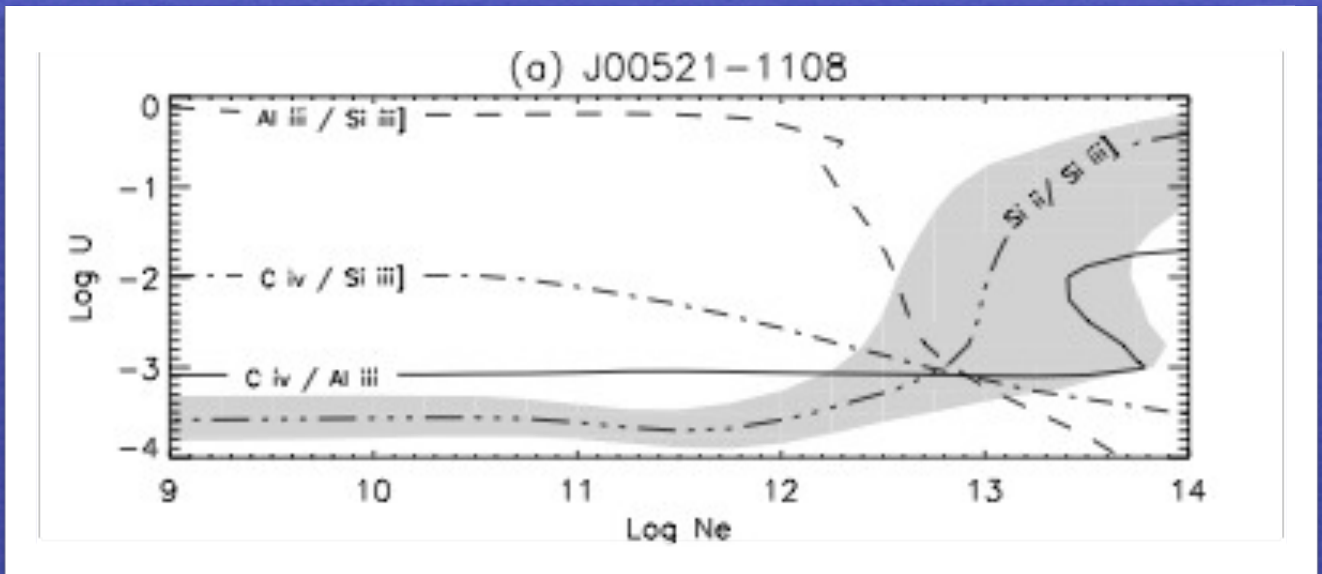

$$\log(n_{\rm H}U) \approx 9.6$$

$$\log(n_{\rm H}U) \approx 9.85$$

$M_{\rm BH}$ for high-z quasars with FORS spectra

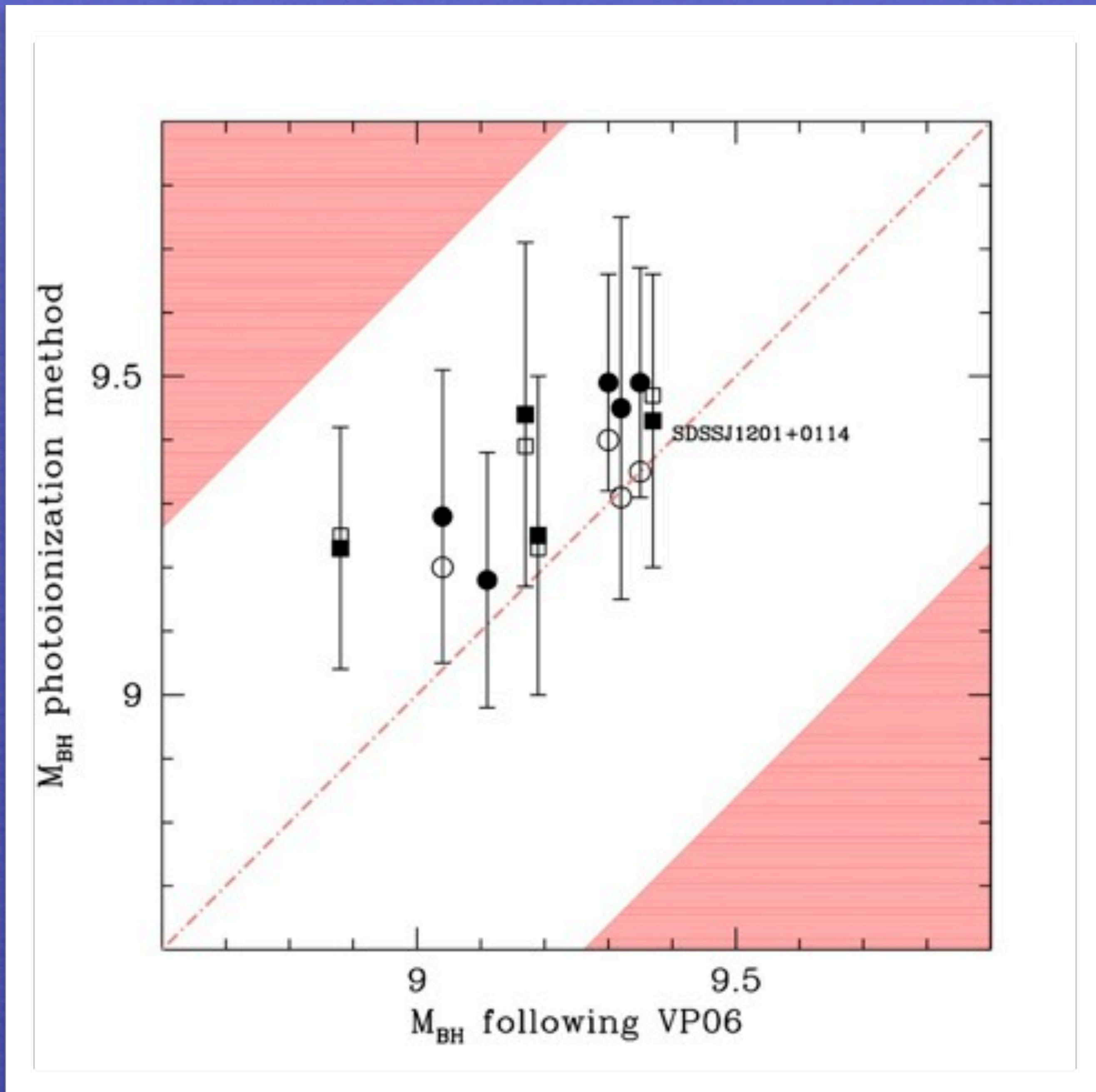

$$\log M_{\rm BH}({\rm C\,IV}) = \log\left\{\left[\frac{{\rm FWHM(C\,IV)}}{1000\ {\rm km\ s^{-1}}}\right]^2\left[\frac{\lambda L_\lambda(1350\text{Å})}{10^{44}\ {\rm ergs\ s^{-1}}}\right]^{0.53}\right\} + (6.66\pm0.01) - s_{\rm f}$$

Vestergaard & Peterson 2006

Comparison with $M_{\rm BH}$ from C IV L correlation

NB: both measures $\propto L^{1/2}$

Negrete et al. 2011, submitted

Sources of concern

fundamental assumptions
photoionization, spherical symmetry
one density, one ionization parameter:
clearly an oversimplification

predicted line intensities
lack of perfect convergence

measurements of line fluxes (S/N, dispersion, deblending)
coarse assumptions on metallicity
continuum shape, anisotropy
all errors in the conventional application
of the virial mass relationship

Conclusions

The described photoionization method:

works best for NLSy1-like sources at high redshift

with ideal dataset allows determination of
density, ionization, and metallicity

works for other sources as far as the (nU) is sought
but reliability difficult to assess

probably lower uncertainty
than method based on the L-$r_{\rm BLR}$ correlation

requires high S/N and moderate dispersion
but can in principle be applied to very high z (>6.5)

Downsizing?

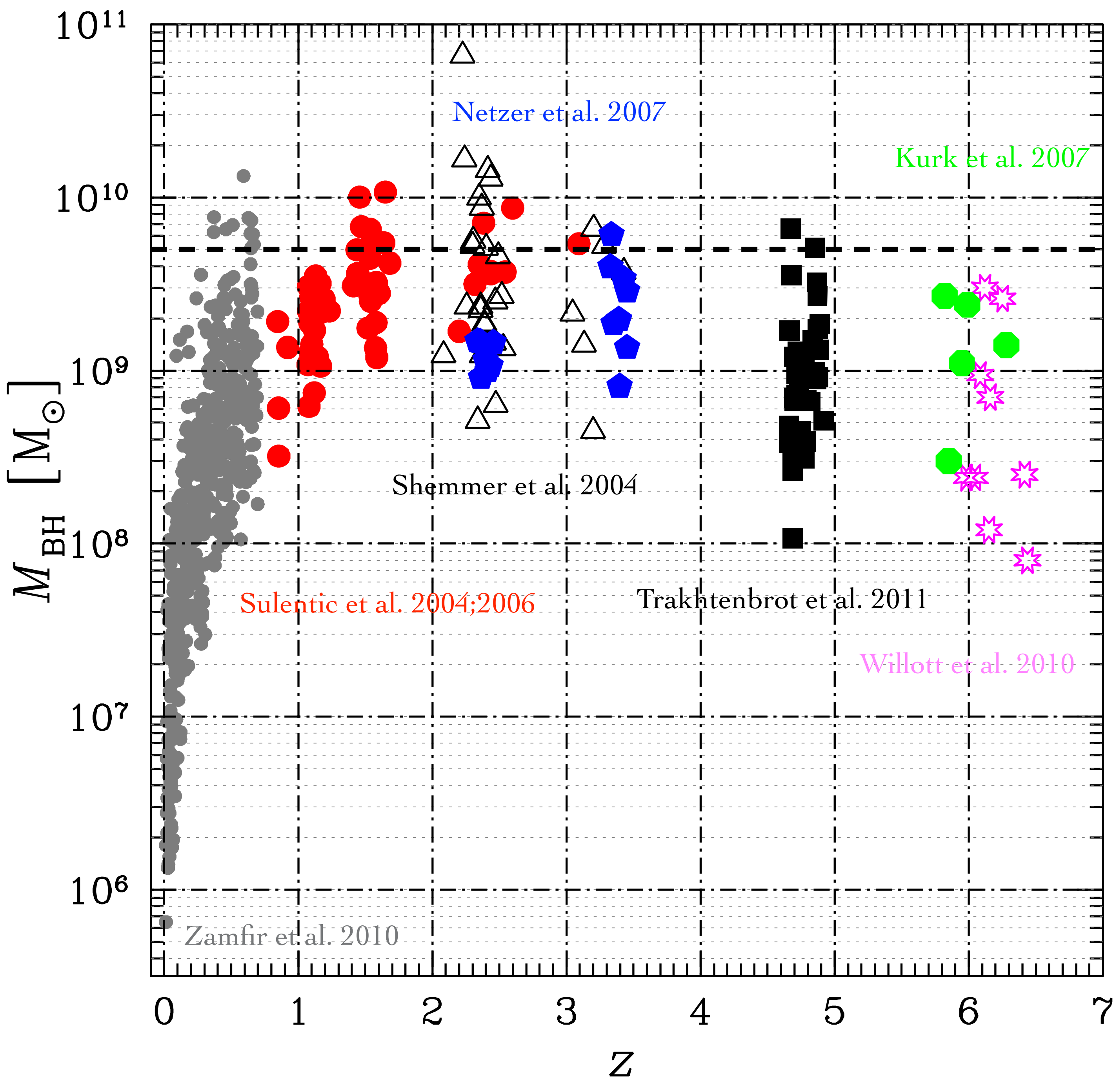

10^{11}
10^{10}
10^{9}
10^{8}
10^{7}
10^{6}
M_{BH} $[M_\odot]$
0
1
2
3
4
5
6
7
z
Netzer et al. 2007
Kurk et al. 2007
Shemmer et al. 2004
Sulentic et al. 2004;2006
Trakhtenbrot et al. 2011
Willott et al. 2010
Zamfir et al. 2010